Internship Report

Nanostructuring of Hexagonal Boron Nitride: Capabilities & Limitations of Patterning with Thermal Scanning-Probe Lithography

Author

D. N. Maaskant, BSc

Utrecht University

Supervisors

N. Lassaline, MSc

Prof. dr. D. J. Norris

ETH Zürich

Examiner

Dr. F. T. Rabouw

Utrecht University

Optical Materials Engineering Laboratory
Eidgenössische Technische Hochschule Zürich

June 2021

ETHzürich

The image on the title page shows an optical image obtained in this work after patterning of an hexagonal boron nitride flake.

Abstract

Hexagonal boron nitride (hBN) is a layered semiconducting material that is interesting for photonic and electronic nanodevices due to its favourable properties (*e.g.* high thermo-chemical stability, an atomically smooth surface and a strong emission in the UV). Recently, novel phenomena and functionalities have been reported accomplished by the nanostructuring of hBN containing structures, like localised quantum emission and band structure engineering of graphene. However, current lithography techniques used for patterning of hBN limit device architecture, as they are only able to make binary patterns (*i.e.* patterns with only two depth levels). Thermal scanning-probe lithography (tSPL) could overcome this limitation as it is capable of greyscale patterning (patterning with more than two depth levels). tSPL locally evaporates an organic resist with an atomically sharp hot probe tip after which the pattern is transferred into the underlying surface *via* reactive ion etching. In this work, we employ tSPL and explore its capabilities and limitations for the nanostructuring of hBN. We demonstrate that tSPL can be successfully used for patterning of hBN and confirm the possibility of greyscale patterning of hBN with tSPL. We obtained patterns with a minimum feature size with a full width at half maximum of 40 nm (pattern depth 40 nm), resolutions down to ~100 nm (pattern depths of 45 and 65 nm) and we reproduced the targeted pattern with a root-mean-square error as low as 10 nm (pattern depth 45 nm). Upon decreasing the size of the targeted features and increasing the pattern depth the quality of the patterns decreased, indicating the tip shape as the possible limiting factor for the quality of the pattern. Further research to determine which pattern step is limiting for the quality of patterning hBN, will enable optimisation of the method. Future research should focus its efforts on the capabilities and limitations of employing tSPL for greyscale patterning of hBN specifically. Nevertheless, tSPL was already shown to offer a successful route towards greyscale patterning of hBN. Therefore, an increased freedom in the device architecture of hBN containing nanodevices is enabled.

Table of Contents

1. Introduction

Hexagonal Boron Nitride (hBN) is a layered dielectric semiconductor with interest for its use in electronic and photonic nanodevices due to its favourable properties. The material consists of alternating nitrogen and boron atoms organised in a hexagonal structure similar to graphene. The in plane bonding is covalent, while the layers are kept together by Van der Waals bonding (VDW bonding). As VDW bonding is relatively weak, it is easy to separate layers using *e.g.* mechanical exfoliation, resulting in a quasi 2D material. Furthermore, properties of hBN include a high thermo-chemical stability, an atomically smooth surface and a strong emission in the UV, making it an excellent material for the use in electronic and photonic (nano)applictions.[1–3]

Structures containing hBN often are VDW heterostructures (*i.e.* different materials layered on top of each other bound by VDW forces). For example, hBN is reported as an ideal substrate for graphene, because it reduces chemical reactivity, surface roughness and intrinsic doping compared to other substrates like SiO_2.[2] In addition, hBN is used to encapsulate materials with the purpose of stabilising the structure.[2,4] Other applications of hBN are IR nanophotonics, ultraviolet emitters and single photon emitters (SPEs).[1] Recently, advancements have been made by patterning hBN and hBN based nanostructures. For instance, Jessen *et al.*, patterned an hBN|graphene|hBN VDW heterostructure enabling bandgap engineering of graphene[5] and Ziegler *et al*. patterned holes into hBN resulting in the localisation of SPEs.[6] Thus, hBN is a promising material for optoelectronic applications and tuning properties by patterning of hBN opens up new device design possibilities.

Current methods used for the patterning of hBN include conventional lithography techniques like focussed ion beam milling[6] and electron beam lithography.[5] However, methods like these are limited in terms of resolution due to *e.g* proximity effects.[7,8] Furthermore, these techniques have no depth control over the patterning, *i.e.* they are able only to perform binary patterning. Methods that are capable of greyscale patterning (*i.e.* patterning with more depth levels) at high resolutions could enable further development of hBN based devices. An emerging lithography technique enabling both high resolution and greyscale patterning was introduced by Pires *et al.* in 2010 and is known as thermal scanning-probe lithography (tSPL).[8] tSPL uses a hot probe tip - similar to a probe tip in atomic force microscopy (AFM) - to locally evaporate an organic resist that is coated on a surface. As the probe tip is AFM like, the topography of the pattern can be directly characterised providing *in situ* feedback on the writing parameters (*i.e.* closed loop writing), resulting in an increased pattern precision. After writing into the resist, the pattern is transferred into the underlying surface using reactive ion etching (RIE).[7–9]

Previous works using tSPL showed that lateral resolutions down to 10 nm are obtainable for shallow depths (a few nanometres), which is explained by the small size of the tip and the absence of proximity effects.[8,10] In addition, precise depth control of the probe tip is possible, enabling greyscale patterning with a precision in the vertical direction of ~1 nm.[11] These capabilities can be used to create improved nanodevices. For example, Lassaline *et al*. take advantages of the capabilities of tSPL: By patterning wavey surfaces as (optical) gratings they improved the grating quality compared to binary gratings,[12] which illustrates how greyscale patterning with tSPL can be used to improve nanodevices. Thus, using tSPL on hBN nanostructures could facilitate improvement of hBN based (nano)devices.

In this work, we explore the capabilities and limitations of tSPL as a method to enable precise and (greyscale) nanostructuring of hBN. Firstly, series of square hole arrays and a fractal pattern containing different depth levels (the Mandelbrot set) were successfully patterned into hBN using tSPL. Subsequently, the patterns were evaluated in terms of several quality characteristics: the resolution (half-pitch), minimum feature size (full width at half maximum) and the overall pattern quality (root-mean-square error between targeted and experimental pattern). We found a minimum feature size in

the fractal pattern with a full width at half maximum of 40 nm at a depth of 40 nm, corresponding well to the shape of the tip. Furthermore, we managed to pattern with resolutions down to ~100 nm in the square hole array patterns for depths of 45 and 65 nm. In addition, the overall patterning quality of the square hole arrays was found to reach root-mean-square errors below 10 nm. When the depth and targeted width of the holes were increased, the overall patterning precision decreased, indicating the shape of the probe tip possibly is the limiting factor. Thus, we found that tSPL can be used to successfully pattern hBN and is a useful method for greyscale patterning of hBN.

In this report, firstly an overview of the relevant background information is given in the Theory section (section 2). Secondly, the methods used for the patterning of hBN and the characterisation of the patterns are provided in section 3. Thirdly, a discussion of the analysis of the Mandelbrot set & square hole array patterns is provided in section 4. Finally, a summary of the main findings and an outlook are given in section 5.

2. Theory

2.1 Hexagonal Boron Nitride

Hexagonal Boron Nitride (hBN) is a layered dielectric material that is often used as quasi 2D material in electronic and photonic devices. It is an indirect bandgap semiconductor ($E_{bandgap} \approx 5.96$ eV) with a crystal structure similar to that of graphene (*i.e.* hexagonal or honeycomb structure) and an atomically smooth surface. The molecular structure of hBN is shown in Figure 1, consisting of layers (~ 0.33 nm thickness per monolayer) of alternating boron (blue circles) and nitrogen (yellow circles) atoms. As a result of the large electronegativity difference between boron an nitrogen, the stacking of the hBN layers favours AA' stacking, where electron deficient boron and electron rich nitrogen atoms are stacked directly below or above each other. The layers are held together by Van der Waals forces, making it relatively easy to separate layers from each other, *e.g.* mechanical exfoliations is often used to extract layers of hBN. The in plane bonding between the boron and nitrogen atoms are covalent as they are sp^2 hybridised, similar to graphene. However, due to the large polarity of the bonding between boron and nitrogen the bonding is partially ionic, which reduces the covalency end electrical conductivity (in contrast to graphene, which is highly conductive). As a result of the in plane bonding, hBN is expected to be relatively free of dangling bonds. In addition, hBN was shown to be very stable and chemically inert.[1–3] Due to its favourable properties many research efforts are put into implementing hBN as nanomaterial in photonic and electronic devices at the nanoscale.[1,2] To further illustrate the great potential of hBN for implementation in nanotechnology, hereafter some examples of research efforts and applications will be discussed.
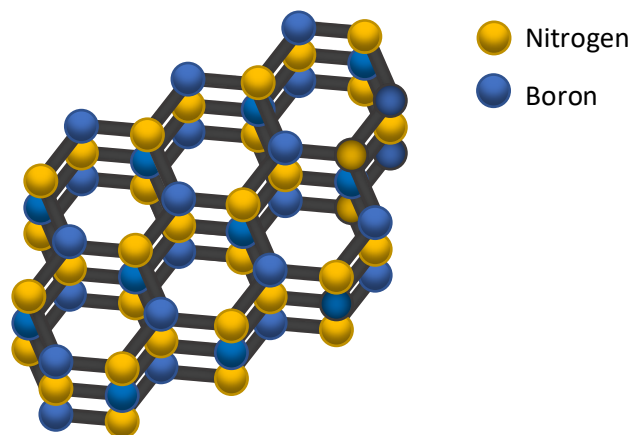
Figure 1: The molecular structure of hBN, consisting of hexagonal structured layers with equal composition of alternating boron and nitrogen atoms (blue and yellow circles respectively).

2.1.1 Hexagonal Boron Nitride for Applications and the Role of Patterning in Advancements

hBN is used for both electronic and photonic devices, either as stabilising material or for its intrinsic properties (*e.g.* strong emission in the UV and an atomically smooth surface as discussed above). In addition, nanostructuring of hBN enables the engineering of its properties for specific applications.

hBN is reported as an ideal substrate and encapsulating material in Van der Waals heterostructures (VDW heterostructures), due to its stabilizing properties and similar crystal structure to graphene.[2,4] For example, using hBN as a substrate for graphene in electronic devices instead of SiO_2 improves carrier inhomogeneity and mobility by almost an order of magnitude and reduces chemical reactivity, surface roughness and intrinsic doping.[2] In addition, the advantage of using hBN in VDW heterostructures goes beyond stabilising. According to theoretical (first-principle) calculations the electronic structure of graphene|hBN bilayers can be tuned.[13] Experimentally, it was shown that creating super lattices by patterning periodic holes into hBN|graphene|hBN structures enables band

structure engineering of graphene. In this case, the stabilising effects of hBN on the structure resulted in the possibility of engineering the band structure while maintaining ballistic transport (*i.e.* unimpeded flow of charge carriers over a relatively long distance).[5] A schematic representation of the super lattice containing structure is shown in Figure 2a.

Furthermore, hBN is widely applicable in photonic devices, *e.g.* for IR nanophotonics, as ultraviolet emitters, in VDW heterostructures and as single-photon emitters.[1] For example, the advantage of hBN and the patterning thereof is illustrated when looking at single-photon emitters. Single-photon emitters (*i.e.* quantum emitters) are highly desirable for numerous optoelectronic applications, *e.g.* quantum computing, cryptography and imaging.[14] The presence of single-photon emitters in quasi 2D materials enables the design of new applications, *e.g.* implementation in nanophotonic on a single chip.[15] Extremely efficient single-photon emission in 2D materials at room temperature (in contrast to cryogenic temperatures) was first found in hBN.[15,16] Single-photon emission is hypothesized to originate from defects present at the edges of the material and defects resulting from strain.[6] An example of a method to create single-photon emission is depositing hBN layers on a substrate with nanopillars, inducing curvature and with that straining the hBN layers.[14,17] Furthermore, by using lithography to pattern holes into hBN, Ziegler *et al.* managed to successfully localise single-photon emission. The localisation of single-photon emission is an important step towards integration of single-photon emitters in optoelectronic devices.[6]

Thus, the patterning of hBN enables further engineering of the properties needed for applications. However, currently the design of hBN based devices is limited by lithographic techniques capable only of binary patterning (*i.e.* only one depth level at the time can be patterned into the material). Further freedom in design and thus improvement in hBN based devices can be accomplished by enabling patterning with different depth levels in one patterning run (*i.e.* greyscale patterning). For example, greyscale patterning could enable more control over the curvature of hBN leading to increased control of single-photon emission.

In this work, thermal scanning-probe lithography (tSPL) is explored as a possible technique for greyscale patterning of hBN. A theoretical background on patterning with tSPL will be provided in section 2.3. Firstly scanning-probe microscopy (SPM) will be discussed (section 2.2), because it forms the basis for tSPL and is also important for the characterisation of patterned surfaces.
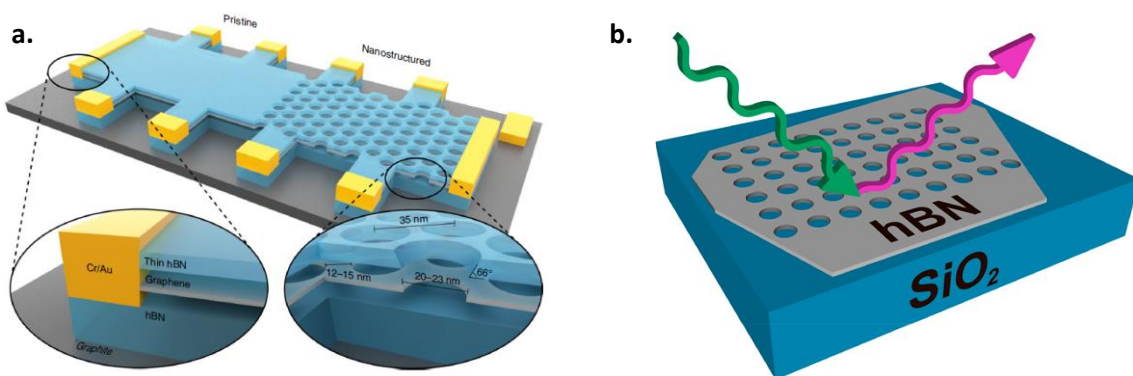
Figure 2: Examples of patterned hBN containing devices. a. Schematic representation of nanostructured superlattice in VDW heterostructure with graphene and hBN, enabling the band gap engineering of the graphene while maintaining ballistic transport. Reproduced from Dean *et al.*[2] b. Schematic representation of nanostructured hBN enabling the localisation of single photon emission. Reproduced from Ziegler *et al.*[6]

2.2 Scanning-Probe Microscopy

With an increased interest in nanomaterials and nanostructures, imaging techniques with sufficient resolution are becoming more important. Techniques available for imaging at the nanoscale include *e.g.* electron microscopy (EM) and scanning-probe microscopy (SPM). SPM is a powerful and unique tool in nanomaterials science as it can both image and structure surfaces at the nanoscale or - depending on the specific technique - even atomic scale. To enable imaging at such a small scale, SPM techniques make use of an atomically sharp probe tip to scan a grid of points on a surface (hence the name *scanning-probe* microscopy). Depending on the SPM technique different interactions between the probe tip and the sample are detected (*e.g.* tunnelling current or force). The detected interactions are mapped and usually presented in an image. The interaction between the probe tip and the surface is used as contrast and determines the measured signal.[18] Additionally, when the interaction between the surface and probe tip are sufficiently strong, it is possible to manipulate the surface, which is an important fact elaborated on in section 2.3.

Historically, the first SPM technique is scanning tunnelling microscopy (STM) which uses the tunnelling current between the probe tip and the surface as contrast. As the tunnelling current is exponentially dependent on the distance between atoms and the probe tip, STM enables imaging at the atomic scale. In addition, STM enables building up structures atom by atom as individual atoms can be moved using the tunnelling current. Furthermore, scanning tunnelling spectroscopy (a deviation from STM) is capable of probing the local density of states (*i.e.* electronic structure) of atoms and molecules. Thus, when electronic information or structural information on the atomic scale is desired, STM is a powerful technique. However, STM requires a high vacuum and the surface needs to be conductive because the tunnelling current is used to obtain signal.[18]

Another SPM technique is atomic force microscopy (AFM) based on the force interactions between the surface and probe tip. It is a powerful and non-destructive technique to obtain high resolution structural and geometrical information, which does not require a conductive surface and does not always requires vacuum.[18] In this work, AFM is used for the surface characterisation of patterns written on the nanoscale. Additionally, a modification of AFM is used to write patterns (scanning-probe lithography, section 2.3). Therefore, the basic working principle of AFM and how to interpret AFM data correctly are elaborated on hereafter.

2.2.1 Atomic Force Microscopy

Atomic force microscopy is an SPM technique taking advantage of the force interactions between the sample surface and an atomically sharp probe tip. A simplified schematic representation of an AFM with its basic components is shown in Figure 3a. An AFM works by raster scanning the surface with the probe tip mounted on a cantilever. A scanning electron microscopy image of a cantilever with probe tip is shown in Figure 3b. The lateral motion to scan the surface is performed using a piezoelectric actuator (piezo scanner), *i.e.* an actuator made of a piezo material in which an applied voltage results in mechanical displacement in the crystal structure. The displacement of a piezoelectric actuator can be controlled up to sub-angstrom precisions. Upon scanning the surface the cantilever responds to force changes between the probe tip by deflecting. The deflection is monitored using a laser beam reflected from the back of the cantilever to a photo diode detector (*i.e.* a cantilever deflection sensor). Usually, the probe tip and sample interaction is kept constant, which is realized by connecting a feedback circuit to the cantilever deflection sensor. The amount of feedback required to maintain a constant interaction at a specific point in the raster is used as a measure of the height of the surface at that point. Subsequently, the obtained height information at each point is used to reconstruct a topographical map, containing 3D information of the surface.[18–20] An example of the use of AFM is to obtain topographical information on surfaces after patterning them, such as the topography map of a thermochemical nanopatterned surface as shown in Figure 3c.[21] A more detailed explanation on the

fundamentals of AFM and factors needed to be taken into account for data processing are given hereafter.

2.2.1.1 Forces Contributing To The Sample-Tip Interaction & Operation Modes

The force between the probe tip and surface is used as contrast for imaging with AFM. Therefore, it is important to understand which forces contribute to the sample-tip interaction. The contributing forces consist of both long range attractive forces (*i.e.* van der Waals force) and short range repulsive forces (*e.g.* Pauli repulsion and chemical bonding forces) and are dependent on the sample-tip distance. The Lennard-Jones potential is often used as a model for the interactions, describing the potential $U_{LJ}(r)$ caused by the interaction between two neutral atoms at distance, r and contains a term for the attractive interaction and repulsive interactions:

$$U_{LJ}(r) = \left[\left(\frac{R_a}{r}\right)^{12} - \left(\frac{R_a}{r}\right)^6\right],$$

with U_0 corresponding to the depth of the potential well and R_a the distance at which $U_{LJ}(r)$ equals zero. In Figure 4 the Lennard-Jones potential is plotted (red), where the repulsive scales part with $\frac{1}{r^{12}}$ (blue line) and the attractive forces scale with $-\frac{1}{r^6}$ (green line). Originally, the Lenard-Jones model is used to for the interaction between two neutral atoms, however it describes the basic features of the sample-tip interaction as well. For large distances between the probe tip and sample (r is large) the interaction is attractive. The interaction becomes negligible when the probe tip is very far away from the sample surface (r is very large). For small distances between the sample and probe tip (r is small) the interaction is repulsive. This regime in the Lennard-Jones potential is non-monotonously dependent on the distance, r, resulting in two possible sample-tip distances for each attractive force (except at the minimum). Therefore, it is important to choose a side of the minimum and ensure the sample-tip distance remains on that side of the minimum when measuring in the attractive force regime.[18]
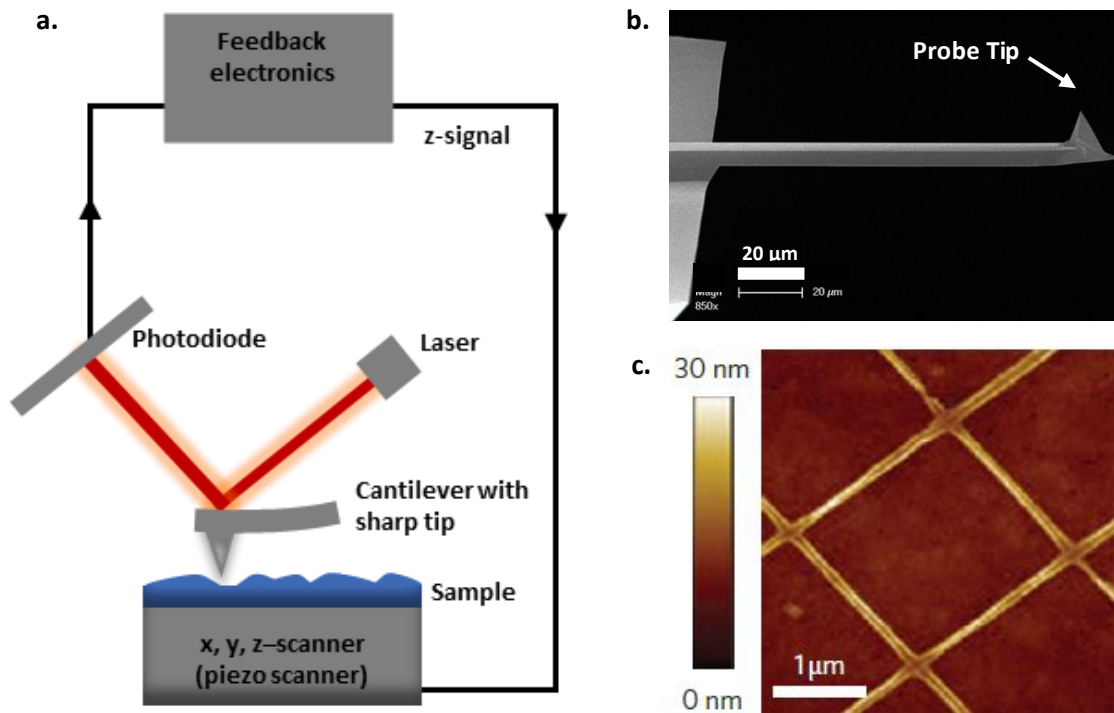
Figure 3: a. Simplified schematic of an AFM setup with its basic components. b. scanning electron microscopy image of AFM cantilever with probe tip. Adapted from Bruker.[22] c. Example of a topographical map containing 3D information (AFM image) of a thermochemical nanopatterned surface. Reproduced from Fenwick *et al.*[21]

$$U(r) = 4U_0 \left[\left(\frac{R_a}{r}\right)^{12} - \left(\frac{R_a}{r}\right)^{6} \right]$$
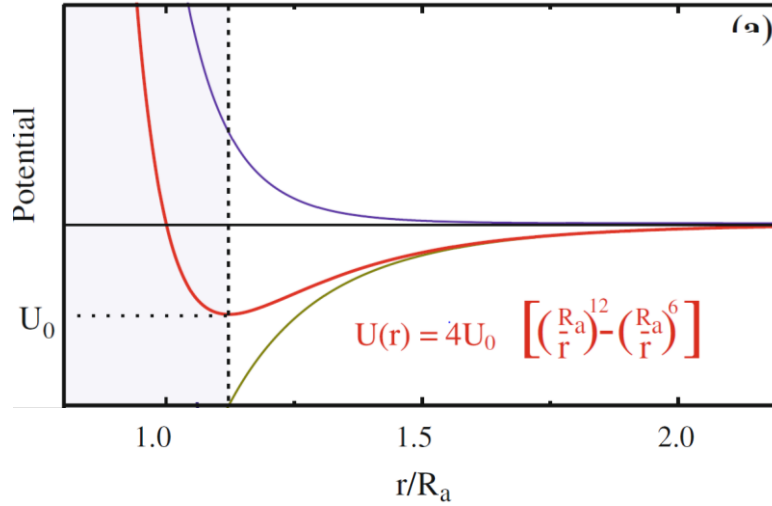
Figure 4: Plot of the Lennard-Jones potential (red) where the attractive forces scale with $-\frac{1}{r^6}$ (green) and the repulsive part scales with $\frac{1}{r^{12}}$ (blue). Adapted from Voigtländer.[18]

a. Contact mode   **b. Non-contact mode**   **c. Tapping mode**
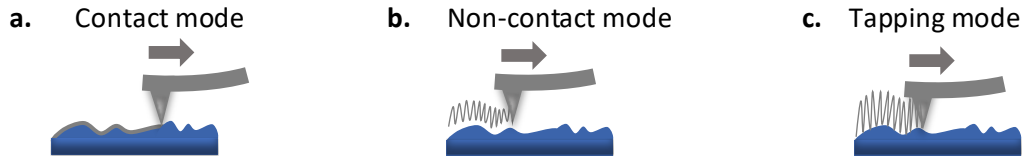
Figure 5: Schematic illustration of the probe tip and surface in the different modes of operation: a. contact mode where the deflection of the cantilever is kept constant, b. non-contact mode where the frequency and amplitude of vibration are kept constant and c. tapping mode where the frequency and amplitude of vibration are kept constant. The grey arrow and grey lines indicate the reading direction and the trace of the probe tip, respectively.

The forces can be probed and depending on the force regime, the AFM operates in different modes. There are three main operation modes, *i.e.* the contact mode, the non-contact mode and the intermediate contact mode. These modes operate in the repulsive, attractive and both attractive and repulsive force regime respectively.[18,19] A schematic representation of the working principle in the different operation modes is shown in Figure 5.

In the contact mode of operation the probe tip is in contact with the sample as it scans the surface (Figure 5a). In this mode the force is kept constant by keeping the sample-tip distance constant. To maintain the distance upon topography changes (*i.e.* changes in height of the sample surface) during scanning of the surface, the cantilever responds by bending. The sample-tip force, F_{st}, translates into a deflection of the cantilever. The total force on the cantilever vanishes in equilibrium, therefore the sum of F_{st} and F_{cant} is equal to zero:

$$F_{total} = F_{st} + F_{cant} = 0$$

It follows that F_{st} is equal to F_{cant}, meaning that the response of the cantilever is proportional to F_{st}. As the cantilever acts as a spring, the force on the cantilever – and thus its response – can be described using Hooke's law for springs:

$$F_{cant} = -k\, \Delta z,$$

where k is the (known) spring constant of the cantilever and Δz the deflection of the spring (*i.e.* the cantilever). The vertical position of the piezo element is adjusted to compensate for the deflection and keep the force constant. In the contact mode the position of the piezo element is tracked and used to

reconstruct topography images. Challenges while operating in this mode arise from the contact diameter due to the size of the tip apex (1 to 10 nm), limiting lateral resolution. In addition, the probe tip and sample are in contact, resulting in the risk of damaging soft samples (*e.g.* biological or organic samples).[18,19]

To reduce stress on the sample, the non-contact mode of operation can be used as the probe tip and surface are not in contact in this mode (Figure 5b). Instead, the probe tip is kept above the surface at sufficient distance to remain in the attractive force regime. The cantilever is excited to vibrate at its resonance frequency with an amplitude smaller than 1 nm. Upon a change in force between the sample and probe tip, the resonance frequency of the cantilever changes. A feedback loop is used to maintain a constant frequency of the vibration of the cantilever and therefore a constant force. The feedback needed to maintain a constant frequency is used as a measure for the force and to obtain topographical information. The interaction forces in this mode are small, which contributes to preserving the probe tip sharpness and high resolutions. However, for small distances it is challenging to keep the probe tip interaction in the attractive force regime.[18,19]

The intermittent contact mode (*i.e.* tapping mode) also reduces the stress on the sample. In this mode, the cantilever is excited to vibrate at a fixed frequency close to its resonance frequency (Figure 5c). The amplitude of vibration of the cantilever in the tapping mode is larger compared to the amplitude in the non-contact mode. The probe tip 'taps' the surface, making slight contact with the surface at the bottom of an oscillation. As mentioned before, changes in the force between the sample and the probe tip, modifies the resonance frequency of the cantilever. However, as the frequency of the cantilever vibration is fixed, the changed force causes the cantilever to respond with a change in the vibration amplitude and phase. A feedback loop is used to maintain a constant oscillation amplitude of the cantilever and consequently keeping the force constant. Again, the amount of feedback required to keep a constant force is used to reconstruct a topography image.[18,19]

Thus, the interaction between the probe tip and sample consist of short range repulsive forces and long range attractive forces. These interactions can be modelled with the Lenard-Jones potential. There are different modes of operation (contact, non-contact and intermittent contact mode) working in different force regimes, which all have their advantages and disadvantages. The mode of operation is chosen based on the sample and the requirements for the desired topography information.

2.2.1.2 Artefacts & Image Processing

Depending on the sample and mode of operation atomic resolutions are obtainable with AFM, however the lateral resolution is often decreased by artefacts resulting from processes intrinsic to AFM. In addition, next to artefacts resulting in a decreased lateral resolution, some artefacts can result in a distortion of the measured topography image. Therefore, it is important to be aware of possible artefacts in order to limit them and to reliably interpret features in obtained images. Factors that could cause artefacts are related to *e.g.* the tip shape, sample tilt, noise, the piezo actuator and feedback overshoot.[18,23]

Artefacts resulting from the tip shape are a major cause of artefacts in SPM. When the aspect ratio of the topographic feature is larger than that of the probe tip, the feature is not imaged correctly. The shapes of topographic features in AFM images are always a convolution of the shape of a feature itself and the shape of the probe tip (*i.e.* tip convolution), resulting in broadened topographic features. [18,23,24] The effect of tip convolution on the acquired image is illustrated in Figure 6, where the blue line is a simulation of the topography feature that is broadened as a result of the tip shape.[24] Furthermore, parts of the surface might never be reached as the tip sometimes does not 'fit' in between certain topography features (*i.e.* dead zones).[18] To recover the real surface topography, mathematical deconvolution algorithms have been designed.[18,24] However, the tip shape is often not known and even

if it is known the tip shape changes over the course of a measurement (*e.g.* due to contamination), making reliable deconvolution challenging. Additionally, dead zones cannot be recovered with such algorithms.[18]

Another common artefact arises from the fact that the sample never lies completely flat, but is always a bit tilted. The sample tilt results in a tilt of the complete topography image with a specific slope. Levelling can be done in several ways, *e.g.* by fitting an image profile line with a polynomial and subtracting the polynomial for that line. Subsequently, the average height of the following line is set equal to that of the previous corrected line. Figure 7 shows a cross section through a topography image before and after correction for tilt. When the image presents isolated features on a flat surface, this line levelling may cause artefacts. Either these features need to be excluded from the calculation or a different method needs to be chosen. One such other method that is often used, is subtracting a plane from the image formed between three selected points. This method can be used when the sample presents a terrace with a relatively low background compared to the terrace height. Fitting a plane through the topography and subsequently subtracting the plane from the topography results in a levelled version of the topography.[23]

Noise in AFM can also result in artefacts in measured topographies, therefore it is important to know what causes the noise and how to limit it. In AFM measurements both vibrational noise and electrical noise are present. Vibrational noise arises from building vibrations and thermal excitation of the cantilever (thermal noise). However, thermal noise is usually not the limiting factor of the noise in the cantilever. Furthermore, electrical noise contributes to the noise of the cantilever as the sensor measuring the cantilever deflection experiences electrical noise. By specifically adjusting and tuning the AFM, part of the noise is limited, *e.g.* vibration isolation setups are used to damp building vibrations and electrical noise is limited by thoroughly debugging the electronics (*e.g.* removing ground loops).[18] In some cases, it might be necessary to perform noise filtering on a data set post measurement. An example of a method to filter noise is Fourier Filtering (FFT), after which unwanted frequency components can be identified and removed.[23]
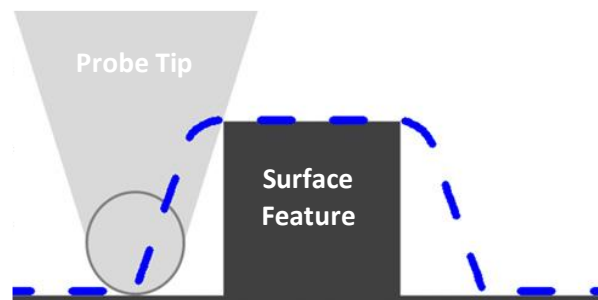
Figure 6: Simulated topography profile (blue) of square feature using a tip with a 10 nm apex, showing the effect of tip-convolution. Adapted from Canet-Ferer *et al.*[24]
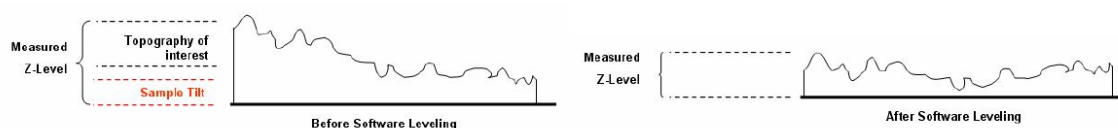
Figure 7: A cross-section through a topography image before (left) and after (right) correction of tilt. Reproduced from Raposo *et al.*[23]

Furthermore, the piezo actuator might cause artefacts like the bending of the structures in the image, which is shown in Figure 8. The bending is a result of piezo creep and non-linearity of the response of the piezo element in the piezo actuator. The change in shape of the piezo material does not complete immediately after the applied voltage. Therefore, the new lateral position is not reached instantaneously after applying a voltage causing bended features in the image. In addition, the response of the piezo element is not the same in both directions due to hysteresis, resulting in differences between images when scanning in different lateral directions.[18]

Lastly, the feedback parameters must be optimised to prevent image artifacts resulting from too fast or slow feedback responses. If the feedback is too fast feedback overshoot might occur when sudden changes in height are encountered by the probe tip, resulting in distorted topography information. If the feedback is too slow the resulting SPM images are blurred.[18]

In summary, AFM is a powerful technique able of obtaining topography images of surfaces with precisions down to atomic resolution. To obtain information on a surface, AFM exploits the force interactions between a probe tip and the surface. Depending on the mode of operation (contact, non-contact or tapping mode) the interaction is tracked in different ways. Often, the feedback required to maintain a constant force as the surface is raster scanned is used to reconstruct the topography image. When taking topography images and interpreting AFM data, it is important to be aware of the possible artefacts and how to limit them. Overall, AFM is a useful technique to obtain topography information from a surface. Furthermore, the AFM setup can be adapted to manipulate surfaces which will be elaborated on in the next section.

Figure 8: An AFM image showing the bending (marked by the arrow) of a step height of a Si surface caused by piezo creep. Adapted from Voigtländer.[18]

2.3 Nanostructuring with Thermal Scanning-Probe Lithography

Many developments in nanotechnology rely on successful fabrication at the nanoscale.[7] A multitude of applications (*e.g.* in nanophotonics and nanoelectronics) depend for their performance on the patterning of materials and surfaces.[7,25] Conventional techniques used for patterning include *e.g.* e-beam lithography, focussed ion beam milling and optical patterning.[5,6,8,25,26] These techniques use electrons, ions and light to pattern a sample or to pattern a resist covering the sample (after which the pattern has to be transferred into the sample). However, these methods are limited in terms of resolution and/or cost effectiveness.[7] Below resolutions of 30 nm proximity effects occur, *i.e.* the area around the intended position to pattern receives a non-zero doze of the beam, resulting in a limited resolution.[8] The limitations in terms of resolution and cost effectiveness have led to the development of different patterning techniques.[7] Scanning-probe lithography which is based on the principles of SPM, is such a technique.

In SPM surface manipulation becomes possible when the interaction between the surface and the probe tip is strong (section 2.2). The formation of a pattern can then be controlled by applying a stimulus to the surface (such as force or heat). Scanning-probe lithography (SPL) takes advantage of this fact, enabling both the patterning and characterisation of a surface.[7,18] A schematic representation of a patterned surface by the probe tip as in SPL is shown in Figure 9. SPL can be divided in two main classes based on which SPM technique underlies an SPL technique. The first class makes use of quantum tunnelling between the probe tip and surface similar to STM, which is known for its ability to perform surface manipulations at the atomic scale. However, the technique requires conductive surfaces and is not cost or time effective.[7,18] The second class of SPL is based on AFM and consists of several subclasses categorized in terms of their driving mechanism used to pattern. Driving mechanisms that are used include electrostatic, thermal, chemical and/or mechanical interactions between the probe tip and the surface. For a lot of these techniques it is possible to perform patterning under atmospheric conditions, which is favourable as it lowers costs and tool overhead. Furthermore, often patterning is done into an organic resist on the surface instead of the surface itself, thus there are no requirements to the type of surface. Therefore, SPL techniques based on AFM are promising to use to pattern materials for applications.[7]

Of SPL methods based on AFM, thermal scanning-probe lithography (tSPL) is particularly interesting as precise control of patterning parameters at nanometer scale and microsecond timescale are possible.[7] tSPL makes uses of a hot probe tip to locally evaporate an organic resist. This method of locally removing resist has advantages over comparable, pre-existing techniques such as plowing and ultrasonic removal of material, as tSPL limits pile up of material and decreases stress on the probe tip. In addition, greyscale patterning is possible with tSPL,[7–9] enabling 3D device architecture design. Figure 10 shows a replica of the mountain Matterhorn (Switzerland) patterned with tSPL by Pires *et al.*, illustrating the greyscale pattern capabilities of tSPL. In this work, the capabilities & limitations of tSPL in patterning of hBN are explored, therefore a more detailed explanation of tSPL is given hereafter.
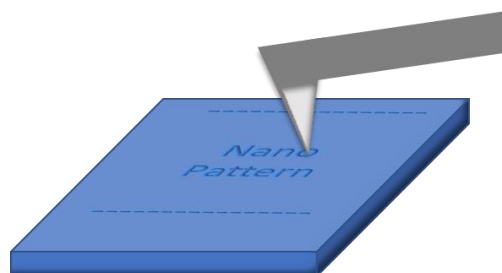
Figure 9: Schematic representation of a patterned surface by a cantilever with probe tip as in SPL, which is both capable of pattering and characterisation.
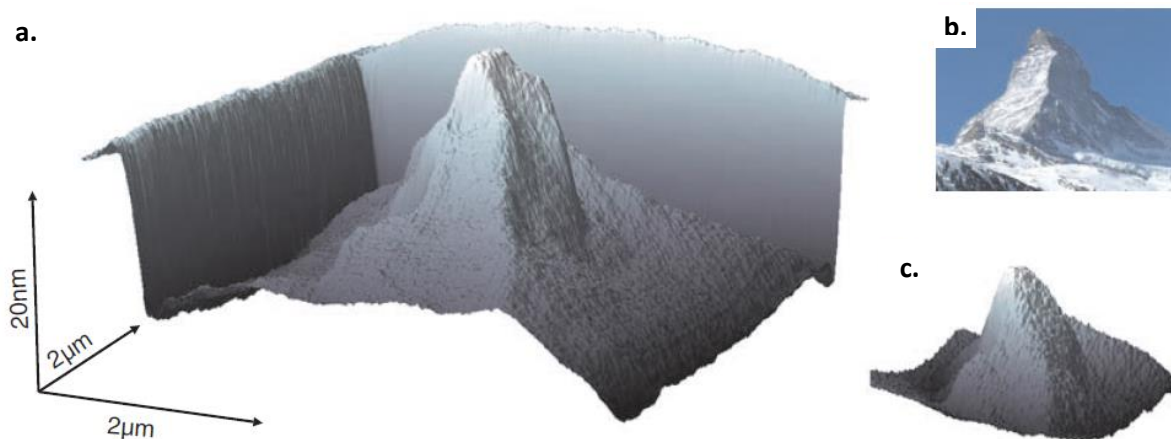
Figure 10: a. AFM scan of a replica of the mountain Matterhorn (Switzerland) patterned into the organic resist with tSPL by Pires *et al*. b. Photograph of the patterned mountain (photographed by Marcel Wiesweg). c. The pattern transferred into silicon. Reproduced from Pires *et al*.[8]

2.3.1 Working Principle & Workflow

The general workflow of tSPL consist of three main steps: coating the surface with an organic resist (I), writing the pattern into the resist with a hot probe (II) and transferring the pattern into the surface (III) (schematically shown in Figure 11). Firstly, the surface is coated with an organic resist for patterning with tSPL. For a resist to be suitable, the molecules should be bound by h-bonds, because they are strong enough to provide stability when handling the sample, but are sufficiently weak to be broken upon thermal activation.[8] Note that when breaking covalent bonds is a part of the patterning it is no longer tSPL, but thermal chemical SPL.[7] Once a suitable resist is chosen, the surface needs to be coated with the resist which is usually done by spin-coating, *i.e.* a small volume of the organic resist is deposited onto the surface after which it is placed in a spinner to evenly distribute the resist.

Secondly, a pattern is written into the resist using a hot probe following the so-called 'closed-loop writing' scheme as schematically shown in Figure 11b. For this purpose, first the desired pattern is programmed as a pixel grid which is loaded into the software of the tSPL setup. Then, the force and temperature stimuli on the cantilever are set depended on the desired depth at each pixel (Figure 12). When evaporation of the resist is required, the tip is brought to the surface, a downward force is applied and the tip is reversibly heated by applying a current into the cantilever legs. The transport of heat is only sufficient to cause evaporation of the resist when the surface and probe tip are in close proximity. Given this fact and the small size of the tip, evaporation of the resist occurs only locally. Subsequently, the probe is cooled-down and performs a back-trace, measuring the topography of the surface as in the contact-mode of AFM. The acquired data functions as a feedback mechanism to adjust the patterning parameters for the next line as needed. The combination of the feedback mechanism and the local evaporation enables patterning with nanoscale precisions.[7–9]

Thirdly, the pattern needs to be transferred from the resist into the surface which is often done using reactive ion etching (RIE) (Figure 11c).[7,8] The resist serves as a protection layer for the surface. The surface will only start to etch as it becomes exposed, which is earlier where the resist is thinner as a result of the patterning. This results in the etching of the surface in the shape of the patterned resist. Another way to transfer the pattern from the resist is by evaporating a layer of material onto the resist and then using template stripping (*i.e.* separating the resist from the desired material). Then, the

resulting shape of the pattern is the reverse from the pattern in the resist.[12] In this work, reactive ion etching will be used as technique to transfer the pattern into the hBN.

Thus, patterning of tSPL consists of three main steps: firstly, the surface needs to be coated with an organic resist. Subsequently, the organic resist is patterned by locally evaporating resist using an AFM like hot probe tip. Then, the pattern in the resist is transferred to the surface underneath.
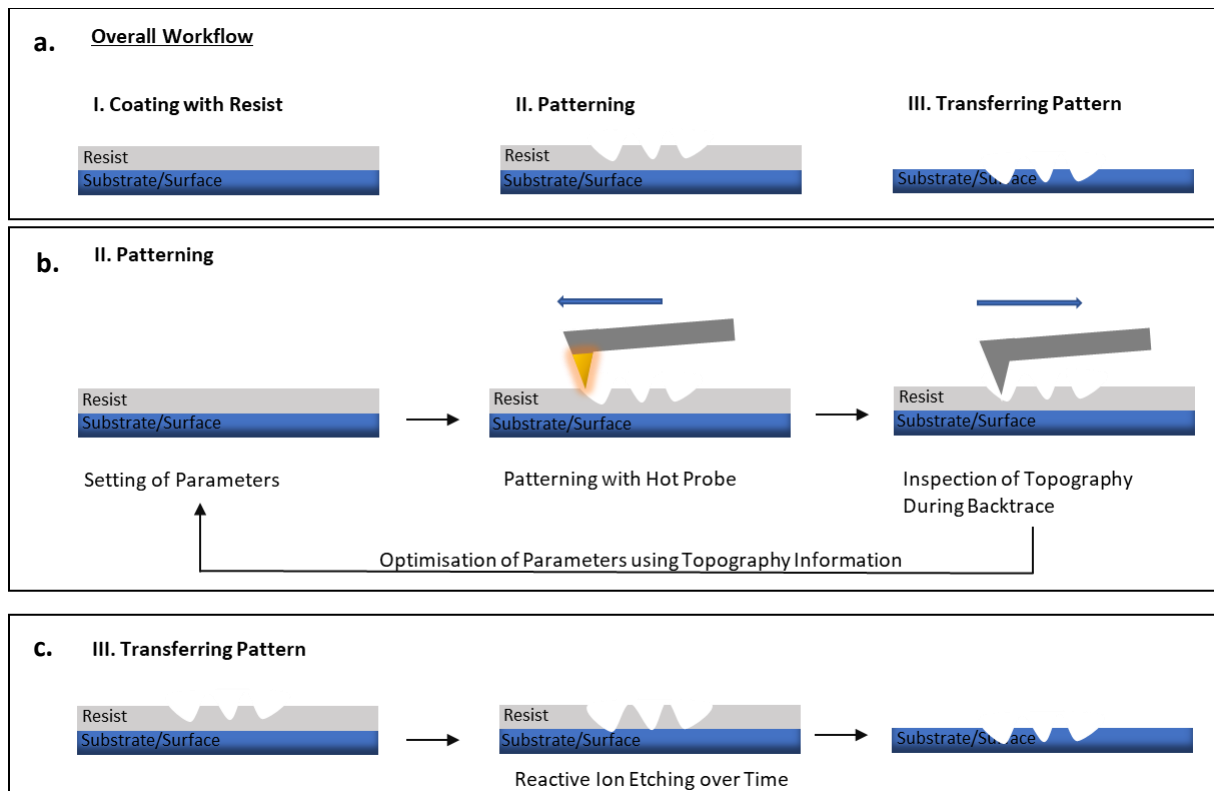
Figure 11: a. The general workflow needed to pattern surfaces using tSPL, where first the surface is spin-coated with an organic resist (I), then the pattern is written into the resist (II) and subsequently the pattern is transferred into the surface (III). b. Closed-loop writing with tSPL: the patterning parameters are set, the resist is patterned with a hot probe tip and after cooling down of the probe tip the topography is measured during a backtrace tip functioning as feedback for the next line. c. The pattern is transferred into the underlying material *via* reactive ion etching.
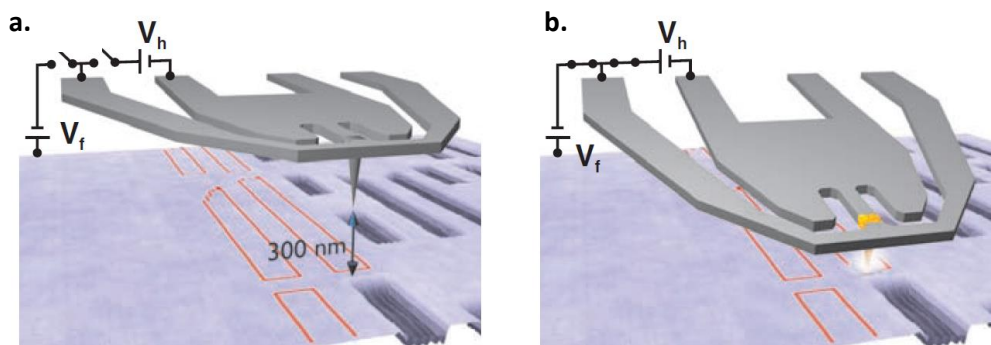
Figure 12: The writing step as was developed by Pires *et al.* in patterning with thermal scanning-probe lithography.[8] The programmed pattern is indicated with the orange outline. a. The cantilever and probe tip are in resting position above the organic resist (in this case 300 nm). b. The tip is brought into contact with the surface of the resist by applying a voltage V_f, meanwhile the temperature is controlled by applying a voltage V_h. By controlling both V_f and V_h at each pixel the programmed pattern is written pixel by pixel. Reproduced from Pires *et al.*[8]

2.3.2 Capabilities & Limitations of Thermal Scanning-Probe Lithography

In this work, we are interested in the capabilities and limitations of using tSPL as lithography technique to pattern hBN. Therefore, it is important to be aware of the advantages and challenges when using tSPL in general. An overview of these advantages and challenges is provided in this section. In addition, the pattern characteristics defining the quality of a pattern are discussed (resolution, minimum feature size and overall patterning precision).

Working with tSPL includes many advantages: Firstly, tSPL works with heat as a stimulus, which works on a wide variety of materials. In addition, no charged particles are used, therefore unwanted cleavage of chemical bonds does not occur and proximity effects are absent (in contrast to *e.g.* electron beam lithography). Secondly, a setup for tSPL is robust, compact and could easily be placed inside a glove box to work under inert environment, while the setup also works under ambient conditions. Furthermore the setup is relatively simple and cost effective compared to focused ion or electron beam systems. Thirdly, the *in situ* capability for topography measurements enables fast characterisation of the patterned surface and closed-loop writing (as explained in the previous section). Due to the capability of *in situ* inspection of the surface marker-less stitching and overlay are possible by locating previously patterned structures before writing. This means it easy to write several patterns together as one. Fourthly, because the force and tip-sample contact can be precisely controlled, greyscale patterning is possible. The precision for the greyscale patterning in the vertical direction is reported to fall within 1 nm.[11,27] The capability of greyscale patterning opens up the possibility to design patterns and nanodevices with an additional degree of freedom.

Next to the many advantages, there are also some challenges when using tSPL as patterning technique. For instance, the throughput is limited by the speed of the movement of the tip: the scan speed of a tip goes only to a few millimetres per second. For comparison, this speed is similar to electron or ion beam lithography operating at their highest resolution (they are faster for lower resolutions). To increase throughput in tSPL, research efforts are put towards the use of several tips in parallel. Another challenge comes with the tip-shape, because the heat transfer is affected by the shape of the probe tip. Over the course of patterning and imaging the tip shape degrades as a result of tip contamination and deterioration caused by friction. Therefore, the cantilever needs to be exchanged on a regular basis to keep achieving high resolution patterning over time.[11]

Furthermore, the capabilities and limitations of a lithography technique are qualified in terms of the highest achievable quality of the resulting patterns with that technique. The quality of a pattern is often determined by quantifying the resolution, minimum feature size and/or overall patterning precision.

Firstly, the resolution is often used to quantify the capabilities of a patterning technique. The resolution is given as the half-pitch (*i.e.* half the period of a feature) of fully separated features.[8,10,28] To obtain information about the resolution limit of a patterning technique, often arrays of equally spaced features are patterned, *e.g.* lines as shown in Figure 13a. The resolution is determined by measuring the complete width of the pattern divided by the amount of features (*e.g.* 2.5 for the pattern shown in Figure 14). Resolutions down to ~10 nm in silicon have been accomplished using tSPL.[10,11] Compared to for example direct write laser lithography, tSPL is more than an order of magnitude better.[11] However, the 10 nm resolution was obtained for a shallow patterning depth of ~2 nm and increasing the depth decreases the resolution,[8,10] because the tip shape influences the shape of the pattern similar to the challenge of tip-convolution in AFM. In Figure 14 the influence of the depth on the resolution as a result of the tip shape is illustrated. To overcome loss in resolution as a result of increased depth, sometimes depth enhancement methods are used after writing into a resit with tSPL.[8,27] One depth enhancement strategy is the hard mask strategy, where the pattern is written into

the resist layer and transferred to a silicon substrate. Subsequently, the patterned silicon substrate can serve as a high quality hard mask for other lithography techniques.[8] With this enhancement technique the depth of greyscale patterns cannot be amplified. An alternative depth enhancement strategy uses etching selectivity (*i.e.* the ratio between the rate of etching the resist versus the underlying surface). When the etching rate in the underlying surface is larger compared to that of the resist, the depth will be amplified.[27] Furthermore, an optimised etching process is important for high resolutions, because over or under etching decreases the quality of the pattern significantly.[10]
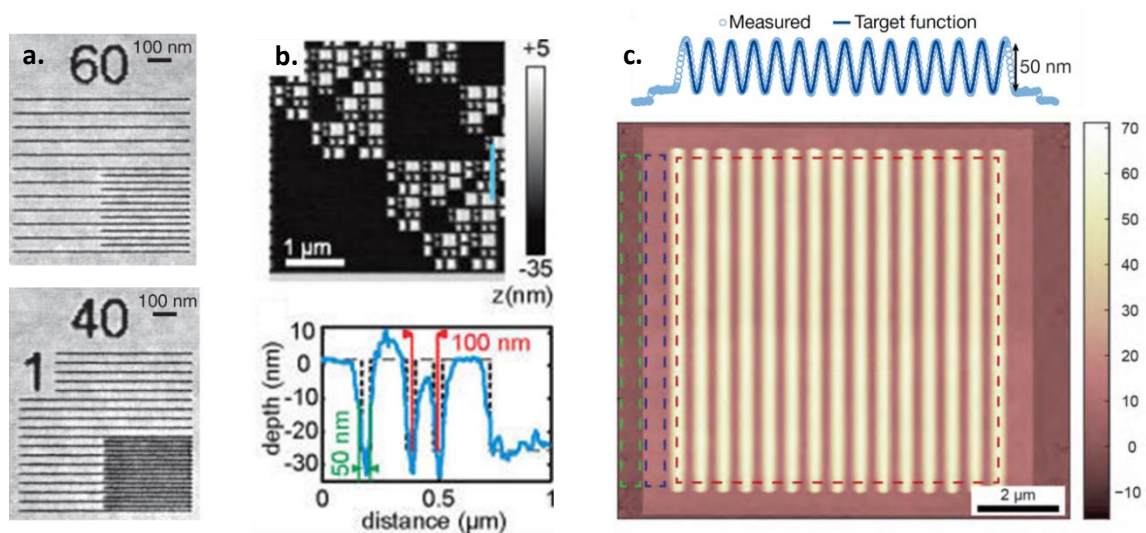
Figure 13: a. Scanning electron microscopy images of lines patterned into silicon used to determine the resolution limit. Adapted from Pires *et al.*[8] b. Topography image of a fractal patterned (top) and cross section through the blue line (bottom) to show a full width at half maximum of 50 nm for a depth of 30 nm. Adapted from Coulembier *et al.*[29] c. Topography image of a wavy surface (outlined in red) with a cross section fitted with a sine function. Adapted from Lassaline *et al.*[12]
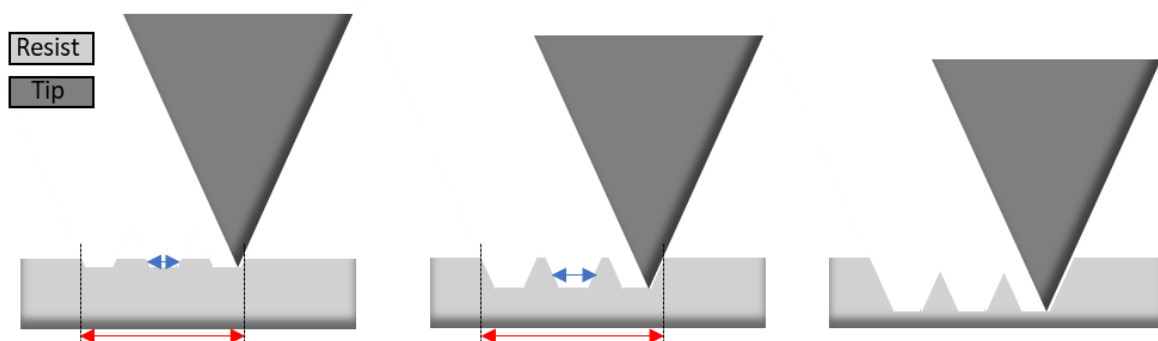
Figure 14: Schematic of a sideview of a probe tip patterning square holes into an organic resist, showing the effect of the tip shape and patterning depth on the resolution and minimum feature size. The resolution is determined by measuring the complete width of the pattern (red arrows) divided by the amount of features (2.5 in this case). The minimum feature size is quantified as the full width at half maximum (blue arrows). As the depth of the pattern increases (left to right), the influence of the shape of the tip increases: the value of the resolution and minimum feature size increase until the holes are no longer fully separated or resolved (right image).

Secondly, the minimum feature size gives important information on the possibilities with a patterning technique. The minimum feature in a pattern is the smallest patterned feature that is still well defined and/or corresponds well to the shape of the targeted feature. Because the patterning depth limiting for resolution due to the tip shape, it is interesting to quantify the minimum feature size related to the depth of the feature. The full width at half max (FWHM) can be used as a parameter to evaluate pattern

quality related to the depth of a feature as shown in Figure 13b.[29] The influence of the patterning depth on the FWHM as a result of the tip shape is illustrated in Figure 14, where the width of the tip has an increasing influence as the depth of the pattern increases. In this work, the FWHM will be used to quantify the size of the minimum feature.

Thirdly, to quantify the overall pattern quality the root-mean-square error (RMS error) can be used. The RMS error is usually used as a measure of the standard diversion between observed values and the prediction value from a model.[30] An example of how this was used to determine the quality of a pattern by Lassaline *et al.* is shown in Figure 13c. The authors patterned a wavey profile with a cross section of a sine function using tSPL and measured the surface topography with an independent AFM. As the cross section of the targeted pattern was a sine function, the surface was fitted with a sine function (amplitude of 25.5 nm and period of 610 nm). The RMS error between the fit and surface was calculated to be 1.7 nm which shows an overall patterning precision over the fitted region as small as 1.7 nm.[12] Alternatively, it is possible to calculate the RMS error between the experimental and programmed pattern without fitting the pattern to obtain a quantification of how well the targeted pattern was reproduced. In this work, we use the latter definition for the RMS error. In Figure 15, a schematic representation of a cross section through a targeted pattern of square holes (blue lines) is shown with the red dots representing a measured experimental pattern. The difference between the targeted depth $\hat{z}_t$ (nm) and the measured depth z_t (nm) at lateral position t (*i.e.* the residual, $\hat{z}_t - z_t$) is a quantification of the deviation of the experimental pattern from the targeted pattern. The root-mean-squared error ($RMS\ error$ (nm)) is the square root of the average of squared residuals, giving a quantification of the overall deviation:

$$RMS\ error = \sqrt{\frac{\sum_{t=1}^{T}(\hat{z}_t - z_t)^2}{T}},$$

with T the amount of data points in the experimental cross section and $\sum_{t=1}^{T}(\hat{z}_t - z_t)^2$ the square of the sum of all residuals from 1 to T.
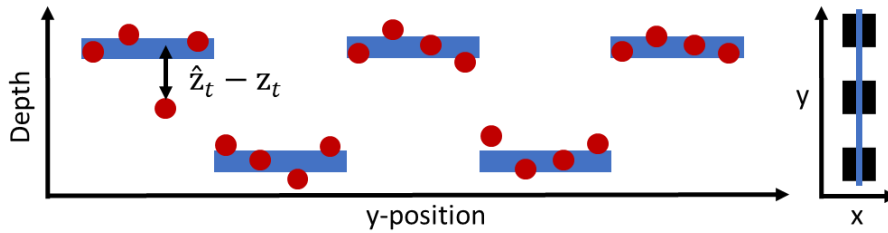
Figure 15: Schematic representation of a cross section (blue) through square holes as a targeted pattern (right side) with the red dots representing a measured experimental pattern. The difference between the targeted depth and measured depth, $\hat{z}_t - z_t$, gives a quantification of how well the pattern was reproduced at a specific point. Using this difference in the definition of the RMS error quantifies the overall patterning precision.

In summary, thermal scanning-probe lithography is a powerful tool that can be used on many materials and overcomes some of the limitations of conventional lithography techniques. High quality patterns can be made using tSPL and its capability of greyscale patterning enables more freedom in (nano)device architecture. In this work, we will explore the capability of tSPL to use on hBN by patterning hBN and analyse the quality of the pattern. The parameters used to analyse the quality of the pattern are the minimum feature size quantified with the FWHM, resolution (half-pitch) and overall patterning quality using the RMS error.

3. Methods

3.1 Materials

4 inch diameter, 1 nm thick silicon (Si(100)) wafers were purchased from Si materials. The polymer resist PMMA/MA (AR-P 617: poly(methylmethacrylate-co-methacrylic acid), 33% copolymer, 3% dilution in anisol) was purchased from Allresist GmbH. Acetone and isopropanol were provided by the Binning and Rohrer Nanotechnolegy Centre (BRNC), IBM Zürich. Hexagonal Boron Nitride (hBN) was purchased from 2D Semiconductors. NCHV-A cantilevers used for AFM were obtained from Burker. The silicon cantilevers (tip radius ~3 - 5 nm) used for tSPL were provided by SwissLitho (now called Heidelberg Instruments Nano).

3.2 Patterning of Hexagonal Boron Nitride

The patterning of hBN was performed using the thermal scanning-probe lithography workflow as described in section 2.3.1. The methods used in this work were adapted from Lassaline *et al.*[12] The main steps to pattern hBN using tSPL are sample preparation (I), spin-coating (II), patterning with tSPL (III) and transferring the pattern into the sample *via* reactive ion etching (IV) (Figure 16). Step II to IV were performed in the clean room of BRNC (IBM Zürich). Hereafter, more detailed descriptions of the main steps are provided.
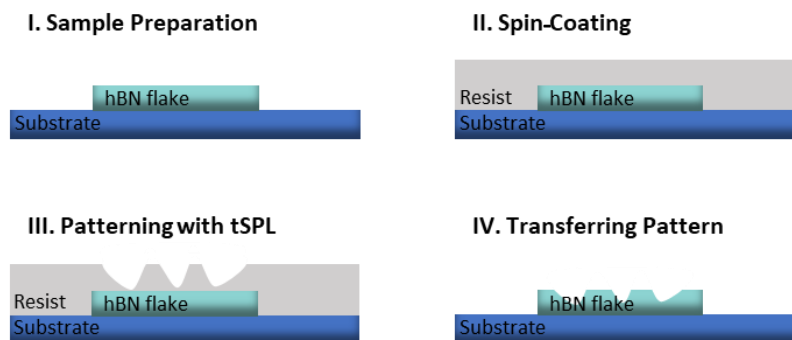
Figure 16: Schematic of the workflow used in this work to pattern hBN. I. Sample preparation consisting of mechanical exfoliation of hBN onto the substrate. II. Coating of the sample with an organic resist *via* spin-coating. III. Patterning of the resist with thermal scanning-probe lithography (tSPL). IV. Transferring of the pattern written into the resist into the underlying hBN flake *via* reactive ion etching.

3.2.1 Sample preparation

Firstly, a silicon oxide (SiO$_2$) layer of 285 nm was thermally grown onto a silicon wafer. The wafer was diced into ~2x2 cm^2 chips, which served as a substrates for the hBN. The hBN was exfoliated onto the substrate (using a mechanical exfoliation procedure), leaving hBN flakes on the chips. Subsequently, an optical microscope was used to locate flakes suitable for patterning based on flake size, thickness and thickness homogeneity estimated based on colour. This is possible as the colours are a result of interference of reflection which is dependent on the thickness of the hBN flakes (as the optical reflectivity of hBN is thickness dependent[31]). Afterwards, to make sure the flakes were suitable for patterning, the thickness of the flakes was checked with atomic force microscopy by measuring the step edge between the desired flake and the substrate.

3.2.2 Spin-coating

The coating of the substrate and sample surface (the chip) with the resist was accomplished using spin-coating. The resist was pipetted onto the chip. Then, the resist was distributed over the complete chip by spinning the chip in two steps: Firstly, the spin speed was brought to (with an acceleration of 500 rpms^{-1}) and kept at 500 rpm for 5s. Secondly, the spin speed was brought to 2000 RPM with a total step time of 40 seconds (an acceleration of 2000 rpms^{-1} was used). After spin-coating the chip was

baked at 180 °C for 5 minutes in order to evaporate the solvent from the resist. The resulting thickness of the resist was ~150 nm, as was checked by scratching the resist (at a location on the chip away from the desired hBN flakes) and measuring the thickness in a line perpendicular over the scratch with a surface profiler (DektakXT, Burker).

3.2.3 Thermal Scanning-Probe Lithography

The method of writing a pattern into the resist was thermal scanning-probe lithography for which a NanoFrazor Explore (SwissLitho) was used. The chip was brought onto the sample stage of the NanoFrazor. The cantilever and probe tip held by the cantilever holder was mounted into the NanoFrazor. Afterwards, the tip was brought in close proximity to the surface of the chip and surface contact was reached using an auto-approach function. Subsequently, a calibration on sample tilt, tip position, and temperature response was performed. Then, the bitmaps of the designed patterns (see section 4.1) were loaded into the NanoFrazor software. Prior to patterning the resist on top of the hBN flakes, calibration scans were performed away from the desired region to optimise pattern quality. After calibration, the tip was brought to a position with an hBN flake. As the tip scanned across a pixel grid (10×10 nm^2 pixels), a variable force pulse of 5 µs was applied at each pixel to evaporate an amount of resist corresponding to the depth given by the bitmap. The maximum depth was set in the NanoFrazor software. The temperature of the tip was set to 1100 °C, expect for the hole arrays with a patterning depth of 65 nm (HA65), where 1000 °C was used.

During the backtrace the topography was measured similar to contact-mode AFM (the tip is cooled down prior to a backtrace), resulting in feedback on deviations between the written and the targeted pattern (closed-looped writing as explained in section 2.3). When necessary, the NanoFrazor adjusted its writing force for the next line based on the feedback. After finishing a pattern, the tip was brought to a different position on the flake or to another flake to write the next pattern. If the shape of the subsequent pattern was significantly different from the previous pattern, new calibration scans were performed prior to patterning at the desired location on top of an hBN flake.

3.2.4. Transferring the Pattern into hBN Using Reactive Ion Etching

The pattern written into the resist was transferred into the hBN *via* reactive ion etching (RIE) (Oxford instruments, PlasmaPro System). The etching was performed with a radiofrequency power of 75 W, a chamber pressure of 40 mTorr and 50 standard cubic centimetres per minute (sccm) of SF6 gas. The duration of the etching was varied per chip and was chosen based on the desired thickness of resist to etch away. After etching the remaining resist was washed by sonicating the chip in acetone for 2 minutes and then in isopropanol for 2 minutes. After these steps, a fast visual inspection on whether the pattern was transferred was performed using an optical microscope.

Note that prior to the etching of the patterned samples, the etching speed was calibrated by etching an empty chip spin-coated with the protocol described in section 3.2.2. The thickness of the resist was determined with the surface profiler both before and after etching of which the difference was then divided by the amount of etching time (etched away thickness/time), resulting in the etching speed of the resist. The etching selectivity (*i.e.* the etching rate of the hBN compared to the resist) is approximately 1:1. The obtained speed was then used to determine the duration of the etching of the patterned samples.

3.4 Characterisation Techniques

3.3.1 Optical Microscopy

Optical images of the hBN flakes were obtained using a Leica light microscope.

3.3.2 Scanning Electron Microscopy

Scanning electron microscopy (SEM) images were obtained using a Hitachi S-4800 electron microscope, with an acceleration voltage of 3 kV measuring secondary electrons and the lower detector.

3.3.3 Atomic Force Microscopy

Atomic Force Microscopy (AFM) scans were obtained using a Dimension FastScan AFM (Burker) with a NCHV-A cantilever (Burker) in tapping mode under ambient conditions. The amount of lines and samples per lines were set such that the pixel sizes were approximately 10×10 nm^2.

3.3.3.1 Data Processing

To limit the effect of artefacts, post analysis data correction and processing is needed prior to using the AFM scans (performed using Matlab version R2020b). The data correction is based on the procedure used by Lassaline *et al.*[12] Figure 17a and b show an example of an AFM scan of a patterned hBN surface before and after data processing respectively. The first step in data correction was median row alignment to overcome scan line artefacts. Secondly, the data sets were corrected for sample tilt (*i.e.* plane levelling was performed) by fitting a plane through the unpatterned part of the surface, after which this plane was subtracted from the data. The plane shown Figure 17c is the plane fitted through the area marked by the red outlines in Figure 17a. After this, further data processing was done by rotating the AFM scans to align the image with the bitmaps corresponding to the pattern using bilinear interpolation (*i.e.* the output pixels are the weighted average of the pixels in the 2x2 neighbourhood). Bilinear interpolation was used over the nearest neighbour method as the latter resulted in artefacts. Finally, the image was cropped to contain only the patterned region.
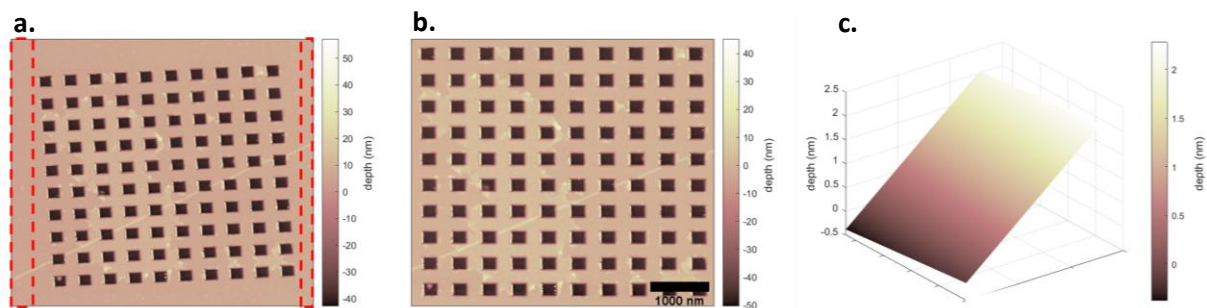
Figure 17: Data processing of AFM scans. a. Image of raw data obtained from an AFM scan of hole arrays patterned into hBN. The red outlines indicate the surface that was used for plane fitting. b. Image of the same AFM scan after data processing (row alignment, plane levelling and image rotation). c. A plot of the plane fitted through the unpatterned part of the surface. This fit was subtracted from the data after row alignment was performed.

4. Results & Discussion

4.1 Pattern Design & Bitmap Generation

To analyse the suitability of the tSPL workflow to nanostructure hBN as described in section 3, several patterning characteristics need to be examined. The characteristics of interest in this work are the resolution, minimum feature size, overall pattern quality (by means of the RMS error) and the ability to greyscale pattern as explained in section 2.3.2. Therefore, patterns that can be used to determine these characteristics need to be designed. Ideally, the patterns are simple and/or mathematically well-defined. To analyse the minimum feature size and test the ability of greyscale patterning of hBN, we use a pattern based on the mathematical Mandelbrot set fractal. Furthermore, we use simple square hole arrays to determine the resolution and overall pattern quality of the patterns.

4.1.1 Mandelbrot Set

The first pattern is designed to contain information on the minimum feature size and to test the capability of the tSPL workflow to greyscale pattern hBN. We define the minimum feature size as the full width at half maximum (FWHM) as discussed in section 2.3.2. To explore the minimum feature size a pattern with features decreasing in size is needed. One type of pattern that both contains features with decreasing size and is mathematically well defined, is a fractal. Fractal patterns are self-similar, *i.e.* similar patterns are present at increasingly smaller scales. Mathematically, fractal sets are models that can be thought of as objects obtained by an infinite recursive process and self-similarity extending to infinitely small scales.[32] However, when physically patterning a fractal there is a limit to the scale of an object (*i.e.* a feature) that can be written. We define the minimum feature size as the FWHM of the smallest feature that is still well defined in the fractal pattern.

We chose the fractal known as the Mandelbrot set, as it contains small features which can be used to analyse the minimum feature size. Additionally, a greyscale can be added to the design enabling the testing of greyscale patterning in hBN. The Mandelbrot set is defined by a set of (complex) numbers, C, for which the function:

$$z_{n+1} = z_n^2 + C$$

does not diverge when iterated. By plotting the boundary between the area of values of C for which the function does and does not diverge (outside and inside the boundaries respectively) the fractal image is generated.[33] We plotted the Mandelbrot set with a limit of maximum 250 iterations and z_n reaching 2 as the criterium for divergence (using Wolfram Mathematica 12). We assigned a greyscale indicating the number of iterations needed for a number in the set C to diverge. This plot was converted to a bitmap (8 bit) of 2000 by 2000 pixels with the lightest colour in the greyscale corresponding to the largest depth (the maximum depth was set in the NanoFrazor software) and the darkest colour (black) the minimum depth (Figure 18a). The pixel size is set to 10 x 10 nm^2 in the NanoFrazor software, resulting in a pattern with a targeted size of 400 μm^2.

4.1.1 Square Hole Arrays

The second pattern is designed to inspect the resolution and overall pattern quality (*via* an RMS error analysis) of patterning into hBN. The resolution is defined as the half-pitch of fully separated features (section 2.3.2), therefore equally spaced features are needed to obtain resolution information on the patterning technique. Accordingly, we designed a simple pattern with equally spaced square holes with a varying size of n by n pixels and a spacing of n pixels. Bitmaps with n equal to 4, 5, 7, 8, 10 and 25 were created using Wolfram Mathematica 12 (Figure 18b). The cross section through the square holes are defined as a square wave with an amplitude of 0.5 times the targeted depth (d) and a period of 2 times n (the targeted hole size + spacing the spacing between the holes):

$$cross\ section = 0.5d * square\_wave\left[\frac{2\pi}{2n}\ t\right] - 0.5d,$$

23

with t the lateral position in the pattern (x or y position depending on the direction of the cross section). Because the maximum of the wave should equal zero, the complete square wave function is subtracted by an amount equal to the amplitude.

After loading the bitmaps into the software of the NanoFrazor, the pixel sizes of the patterns were set to 10 x 10 nm^2, resulting in patterns with targeted hole sizes of 40, 50, 70, 80, 100 and 250 nm^2. The sizes were chosen to contain holes that are still easily patterned and scaled down until it became more challenging to pattern based on pilot experiments (note that this depends strongly on the pattern depth). These bitmaps were used to pattern hole arrays with depths of 45 and 65 nm. Additionally, we use the square hole array patterns to analyse the overall patterning precision (by means of the RMS error) with respect to their size and depth. Note that the pattern used here is binary, even though the main strength of tSPL is greyscale patterning, as this helps analyse the limitations of patterning hBN with the tSPL workflow.
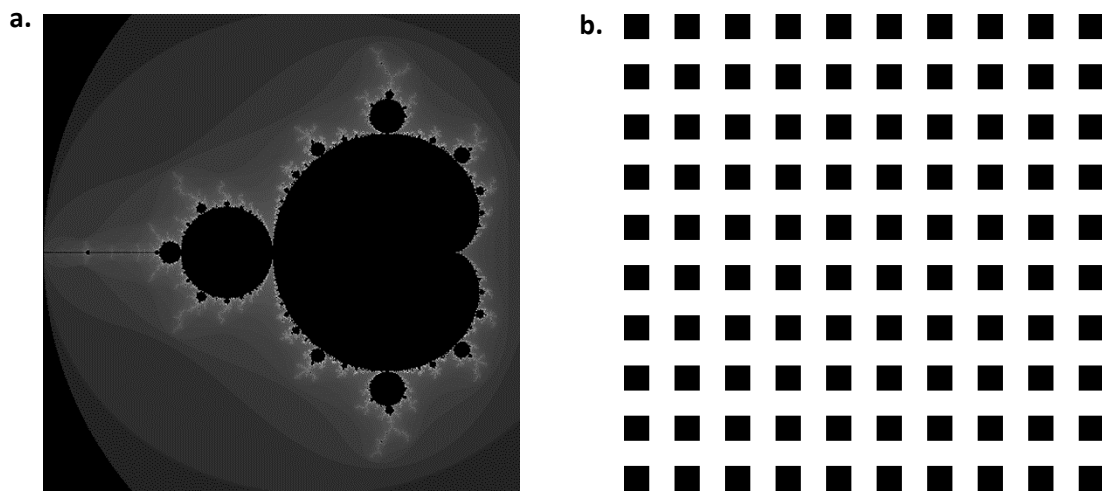
Figure 18: a. Image of the bitmap of a plot of the Mandelbrot set (2000 by 2000 pixels) with a maximum amount of iterations of 250, and the greyscale indicating the amount iterations needed for a number in the set C to diverge. For clarity, the contrast in this image was enhanced. b. Image of a bitmap of square hole arrays with holes of n by n pixels and a spacing of n pixels. Bitmaps with n is equal to 4, 5, 7, 8, 10 and 25 were used.

4.2 Mandelbrot Set Patterned into Hexagonal Boron Nitride

To analyse several characteristics of the capabilities of tSPL, the Mandelbrot set was patterned into the organic resist using tSPL and transferred into the hBN using RIE (see the Methods sections for details on the workflow). The Mandelbrot set pattern was designed to contain different depths to investigate the greyscale patterning of hBN (section 4.1). In addition, the pattern was designed to contain information about the minimum feature size. In this section, AFM measurements are discussed to analyse these characteristics. Prior to the characterisation of the pattern and its features we used optical microscopy as a fast way to check whether the pattern was transferred. The optical image of the hBN flake with the Mandelbrot set patterned into it is shown in Figure 19. The different colours within the flake are indicative of different thicknesses of hBN, as the colours are a result of the interference of reflection dependent on the flake thickness (the optical reflectivity of hBN is thickness dependent[31]). The shape of the Mandelbrot set pattern is clearly visible, thus we concluded that the pattern was transferred into the hBN and proceeded with AFM measurements (section 4.2.1).
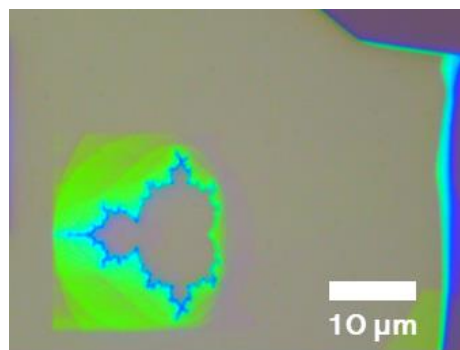
Figure 19: Optical image of the Mandelbrot set patterned into an hBN flake. The different colours within the flakes result from the thickness dependent optical reflectivity.

4.2.1 Surface Topography

To study the Mandelbrot set pattern and its characteristics in more detail, the surface topography of the Mandelbrot set pattern was inspected by taking an AFM scan of the patterned area (Figure 20a). Upon first inspection the written pattern corresponds well to the programmed pattern with the depth gradient present and the dark brown line outlining the border of the Mandelbrot set. However, within the border we also note a discrepancy with the targeted pattern. In this area the depth of the surface was targeted to be homogenous, but we observe an area of the surface that lies slightly (~4 nm, corresponding to ~12 monolayers of hBN) above the targeted depth (indicated with the arrow). It is possible that additional monolayers were already present prior to patterning, as areas with a targeted depth of zero are aimed to remain protected by resist during etching. This means that those areas should not be affected by etching or patterning errors in the resist. However, it is also possible that the sample was over etched. In future experiments, AFM analysis on the hBN flake prior to any patterning steps, would help distinguish between surface features intrinsic to the hBN flake and features caused by patterning.
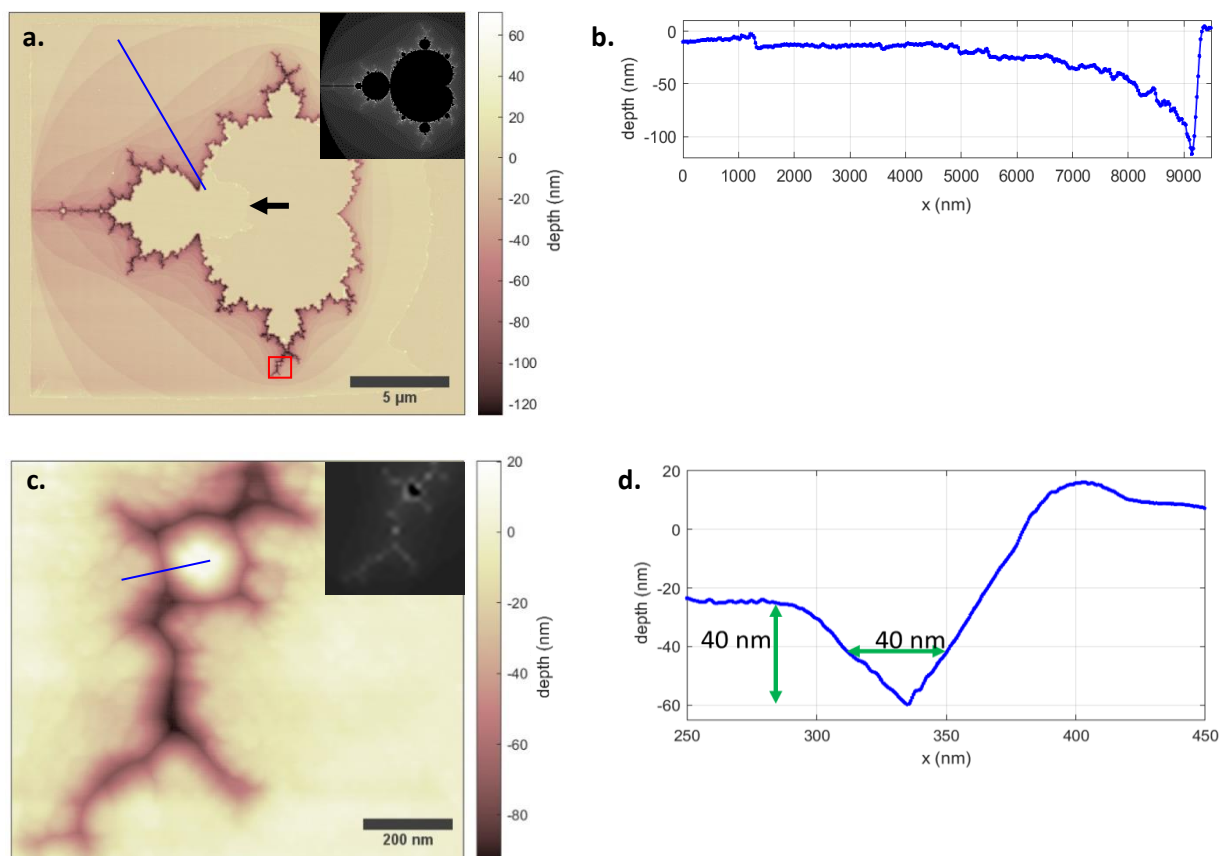
Figure 20: AFM analysis of the surface of the hBN flake after using the tSPL workflow to pattern the Mandelbrot set. a. AFM scan of the Mandelbrot set pattern in the hBN flake. The area outlined with red indicates an area imaged with a higher resolution (shown in c), the arrow indicates an area that lies ~4 nm above the targeted pattern and the inset shows an image of the bitmap of the targeted pattern. b. Cross section through the blue line in a., illustrating different depth levels within one pattern, confirming the possibility of greyscale patterning into hBN. c. AFM scan with higher resolution (0.5 x 0.5 nm^2 pixels) of a small area showing the smallest feature. The inset shows an image of the bitmap of the targeted pattern. d. Cross section through the minimum feature (blue line in c.) with a FWHM of 40 nm for a depth of 40 nm.

4.2.1.1 Greyscale Patterning

By further analysing the topography image of the patterned hBN surface, information about the capability of greyscale patterning into hBN using the tSPL workflow can be obtained. Outside the Mandelbrot set border, the depth gradient representing the amount of iterations before divergence is visible. We took a cross section through the blue line to clearly visualise the different depths within the pattern (Figure 20b). Along this line the pattern contains several depths over a range of 0 to ~120 nm. This result clearly demonstrates the capability of greyscale patterning with tSPL and the successful transferring of different depth levels into hBN. Previously, tSPL has been reported to accomplish depth resolutions down to or even below 1 nm.[11,27] This resolution is theoretically possible for hBN, as the resolution would be ultimately limited by the thickness of hBN monolayers (~0.33 nm). However, to truly explore the limit, a pattern with a depth resolution below 1 nm should be patterned and analysed.

4.2.1.2 The Minimum Feature Size

To analyse the minimum feature size an AFM scan with a higher resolution (pixel size of 0.5 x 0.5 nm^2) was taken of the area outlined in red in Figure 20a. The AFM scan with higher resolution is shown in Figure 20c. In here, again the dark brown line represents the border between the numbers that are and are not contained in the Mandelbrot set. The border forming the smallest object within the Mandelbrot set that is still well defined, is used as the minimum feature size. To quantify the minimum feature size, we took a cross section (along the Mandelbrot set border indicated with the blue line in

Figure 20c) which is shown in Figure 20d. Within this cross section, we obtained a FWHM of 40 nm at a depth of 40 nm. The feature in the targeted pattern is more narrow compared to the written pattern, meaning that there is a limiting step during the overall patterning process. As the shape of the feature corresponds to the shape of the tip used for tSPL (apex of ~5 nm and an angle of 45 degrees), we conclude that the shape of the probe tip used for writing into the resist is likely the limiting factor for the minimum feature size. To support this hypothesis it would be useful to analyse the surface topography of the written resist and compare this to the pattern in the hBN. If the minimum feature size and shape in the resist is the same as in the hBN, this would exclude etching as the limiting step. The topography information obtained by the NanoFrazor is not suitable for comparison, as differences in the images could also be caused by the different mode of operation of AFM imaging.

It should be noted that the shape of the measured features is also affected by tip convolution during the AFM measurement (section 2.2.1.2). To precisely analyse the physical shape of the minimum feature size, deconvolution of the measured topography should be performed in future experiments. However, this is challenging as the algorithm for deconvolution will not recognise the difference between the AFM tip convolution and the influence of the tSPL tip shape on the physical topography, likely resulting in unreliable deconvolution results. To solve this, instead of using a blind tip estimation algorithm, the AFM tip used for measurements could be imaged using SEM. Subsequently, the tip parameters obtained for this image could be used for deconvolution of the topography images.

In summary, we successfully patterned the Mandelbrot set pattern into hBN following the tSPL workflow. We conclude that a greyscale pattern can be transferred into hBN and suggest further experiments to explore the resolution limit into the depth direction. In addition, we found a minimum feature size with a FWHM of ~40 nm at a depth of 40 nm, corresponding well to the shape of the tSPL tip. Therefore, the shape of the minimum feature size is likely primarily limited by the shape of the probe tip used for writing the pattern into the resist.

4.3 Square Hole Arrays Patterned into Hexagonal Boron Nitride

The square hole arrays were designed to inspect the resolution and overall patterning precision *via* the RMS error that can be obtained using tSPL to pattern hBN (section 4.1). Therefore, the square hole arrays were patterned into the organic resist upon the hBN and subsequently the pattern was transferred into the hBN following the workflow as described in the Methods section. Two series of square hole arrays with different depths were patterned: 45 and 65 nm, hereafter denoted as HA45 and HA65 respectively. Note that the depths of the hole arrays were limited and determined by the thickness of the flakes and the duration of the etching, while the written depth in the resist did not correspond to the depth in the hBN (larger depths in the resist).

Prior to characterisation of the surface, we used optical microscopy as fast way to inspect whether the pattern was transferred from the resist into the hBN. Again, the different colours within an hBN flake indicate different thicknesses of hBN, because the dependence on the thickness of hBN for the optical reflectivity. In Figure 20a and b optical images are shown of flakes with the hole arrays HA45 and HA65 respectively. Square patterns are present in the flakes corresponding to hole arrays with a targeted hole size of n by n nm. From this observation we can conclude that the pattern was transferred from the resist into the hBN. Therefore, we performed further characterisation (with SEM and AFM) on the patterns which we used to analyse the patterns, their resolution and the overall patterning precision (RMS error).
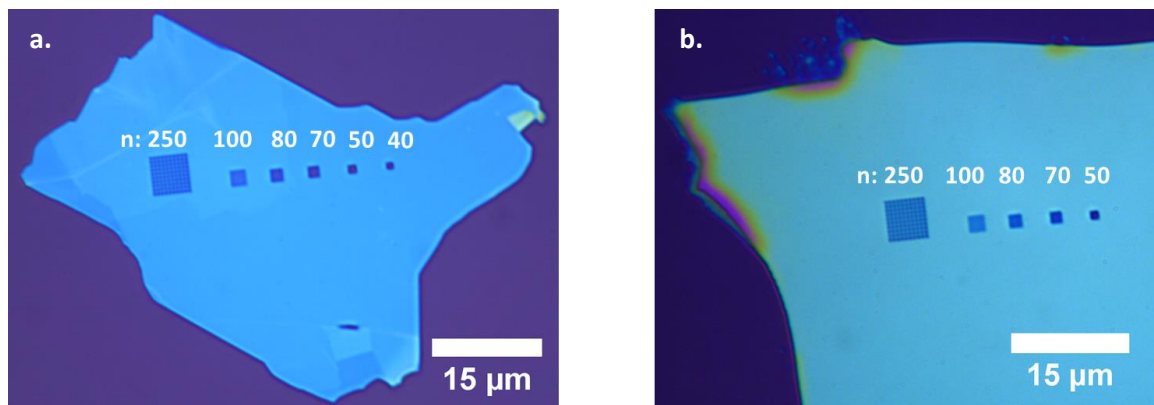
Figure 21: Optical images of square hole array patterns in hBN flakes (blue), with the targeted length of the square holes (n) denoted above the arrays. The different colours within the flakes result from the thickness dependent optical reflectivity. a. Optical image of the square hole arrays with a depth of 45 nm (HA45) and b. the square hole arrays with a depth of 65 nm (HA65).

4.3.1 Resolution

In order to further inspect the patterns and to determine the obtained resolutions, we took SEM images of the hBN flakes with the hole array patterns. In Figure 22 an SEM image of HA45 and HA65 are shown, with the targeted hole size per pattern (n x n nm^2) indicated. In both HA45 and HA65, less contrast is observed on the left side of the holes. This ridges are possibly a result of pile up of resist during the patterning (see section 4.3.2). Within the hole arrays, individual holes can be distinguished for the patterns with a targeted size down to n is 70 for HA45. For HA65 individual holes can be distinguished for the patterns with a targeted size down to n is 100. The difference is likely due to the deeper depth of the pattern in HA65, however the observation could be affected by a decreased resolution due to astigmatism (as the holes seem to have an elongated shape in the x direction). To exclude this, additional SEM images with higher resolution should be made.

As previously discussed, we define the resolution as the half-pitch of the fully resolved features, *i.e.* the half-pitch of the holes in patterns where the individual holes can be distinguished. In addition, we only consider the holes as fully resolved when the targeted depth is maintained, because the highest obtainable resolution is influenced by the depth of the pattern (section 2.3.2). The patterns down to n is 100 nm for both HA45 and HA65 meet the depth requirements (which becomes apparent from the AFM measurements shown section 4.3.2). We measured the pitch of the hole arrays by measuring the complete width of a pattern in the SEM image (using ImageJ) and dividing this by the amount of features (9.5). To be able to visualise the pitches better, zoomed SEM images of the resolved patterns are shown in Figure 23. The resolutions (*i.e.* half-pitches) that were found are ~ 253, 101, 257 and 113 nm for the patterns with n is 250 and 100 for HA45 and HA65 respectively, corresponding well to the targeted half-pitch of n. The resolutions of HA65 are slightly larger compared to those of HA45, which is expected because of the increased depth in combination with the shape of the tip (see Theory section 2.3.2). In addition, the difference is larger for the patterns with smaller holes, indicating that the smaller features are more influenced by the depth.

We note that better resolutions using the tSPL workflow on silicon at shallower depths (10 nm half-pitches at ~2 nm depth) were reported in literature. In addition, other techniques used for patterning of hBN are capable of higher resolutions for larger patterning depths, *e.g.* proximity effects in electron beam lithography only become significant for resolutions below 30 nm where the depth of the pattern has no significant influence.[8] The resolutions with tSPL could be increased by writing the pattern into the resist with shallower depths and adjusting duration of the etching step. This would be especially useful if the depth is indeed limiting due to the tip shape, because in our experiments the depth in the resist was larger than the depth in the hBN (as mentioned above). In addition, analysing and comparing the topography of the shallower patterns in the resist and the pattern transferred into hBN would help distinguish the resolution limiting patterning step. Furthermore, to increase resolutions at larger depths, shallower patterns could be written into the resist followed by depth amplification based on etching selectivity as discussed in section 2.3.2.

In addition, as transferring a greyscale pattern into hBN was shown to be possible (section 4.2), it might be interesting to explore the resolution limit of patterning with the tSPL workflow for greyscale patterns. A possible patterns design could be based on patterns with a cross section of a sine function (similar as used in Lassaline *et al.*[12]) where the amplitude (thus depth) and period (thus pitch) would be varied independently of each other over different patterns. Analysis of series of such patterns with varying amplitude (depth) and period (pitch) would enable to test the resolution limit in greyscale patterns.

Summarising, at least a minimum resolution of ~100 nm is possible using the tSPL workflow on hBN, where the of the probe tip is seemingly the limiting factor which needs to be confirmed with further experiments. We note that higher resolutions would be obtainable by shallower patterning into the resist (and adjustment of the duration of etching) and/or depth enhancement techniques. In addition, for binary patterns other lithography techniques could be used depending in the desired resolution. Furthermore, we suggested experiments to further analyse the resolution in greyscale patterns specifically, as greyscale patterning is the strength of tSPL and greyscale patterning of hBN increases freedom in device design.
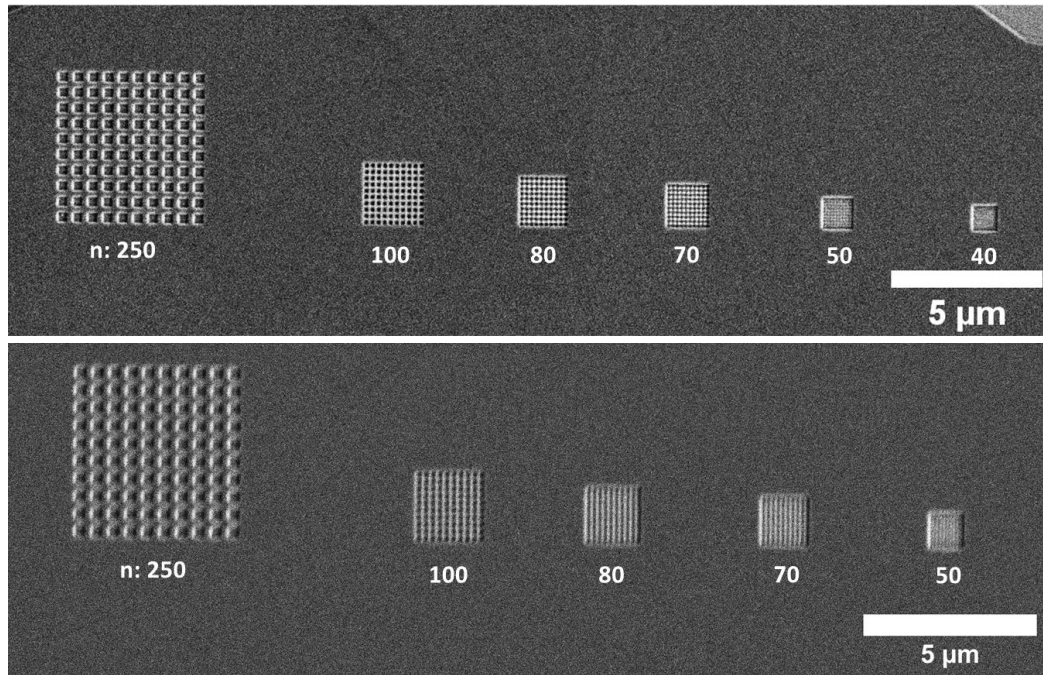
Figure 22: SEM images of the square hole arrays patterned into hBN with different depths, with the targeted length of the square holes (n) denoted below the arrays. a. SEM image of the square hole arrays with a depth of 45 nm (HA45) and b. the square hole arrays with a depth of 65 nm (HA65).
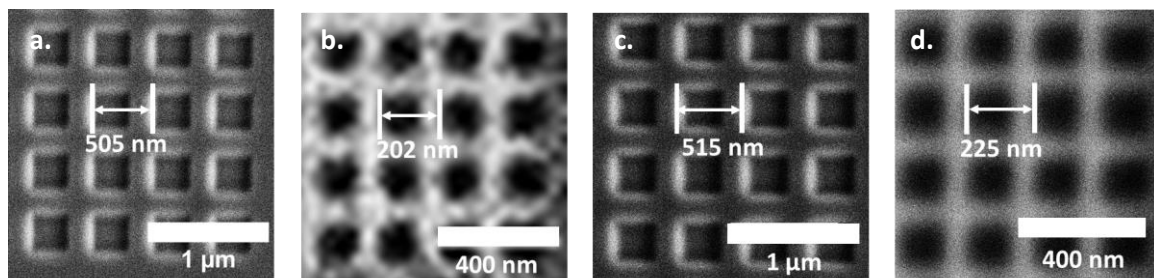
Figure 23: SEM images of right bottom parts of the resolved square hole arrays with their pitch denoted. a. Square hole array with a depth of 45 nm (HA45) and targeted n of 250 nm, with a measured pitch and half-pitch of 505 and 253 nm respectively. b. Square hole array with a depth of 45 nm (HA45) and targeted n of 100 nm, with a measured pitch and half-pitch of 202 and 101 nm respectively. c. Square hole array with a depth of 65 nm (HA65) and targeted n of 250 nm, with a measured pitch and half-pitch of 515 and 257 nm respectively. d. Square hole array with a depth of 65 nm (HA65) and targeted n of 100 nm, with a measured pitch and half-pitch of 225 and 113 nm respectively.

4.3.2 Analysis of the Surface Topography & Root-Mean-Square Error

In order to further analyse the pattern quality, topography information on the patterned surface of the hBN is required. To analyse the pattern quality, we are primarily interested in the fully resolved square hole arrays. Therefore, the focus in this section lies on the hole arrays with a targeted n of 250 and 100 nm. However, for comparison the square hole arrays with a targeted n of 80 nm are also included. In this section, a discussion on the surface topography and the overall patterning quality is provided. Firstly, we discuss the topography images to get an overall impression on the pattern quality and the presence of possible defects. Then, we take cross sections along the holes and compare them to the targeted pattern, using the RMS error to quantify the deviation between targeted and experimental pattern. Finally, we compare the different RMS errors and discuss the observed trends, where we find that the RMS error increases as the holes become smaller and/or the deeper.

4.3.2.1 Surface topography

To analyse the surface topography of the patterned hBN flakes AFM was used. The obtained topography images of HA45 and HA65 are shown in Figure 24. Upon first inspection of topography the images, several observations can be made. Firstly, periodic arrays of holes can be clearly distinguished for the patterns down to a targeted size of 100 nm^2. In contrast, the holes within the pattern with a targeted hole size of 80 nm^2 are no longer fully resolved, though holes in the hBN are still observed.

Secondly, on the left hand side of the holes in HA45 ridges are present similar to what was observed with SEM (section 4.3.1). Ridges like these are sometimes caused by measurement artefacts. However as these ridges were observed in SEM as well, we conclude that they are not artefacts but instead are physically present in the pattern. The ridges could be formed due to pile up of resist during patterning with tSPL, of which the shape was then transferred to the hBN. Within the HA65 patterns less ridges seem present, which could be due to a slightly higher writing temperature (1100 $°C$ instead of 1000 $°C$) resulting in the organic resist to evaporate better.

Thirdly, some undesired irregularities are present throughout the patterns: there are areas of variable size that are higher compared to the rest of the pattern. The irregularities could be a result of the writing process with tSPL, the etching or they could have been present in the hBN itself prior to patterning. In addition, it is possible that the resist was not washed away sufficiently or some contamination is present on the surface. Energy dispersive X-Ray measurements could help determine which elements are present, thus whether the irregularities consist of resist or hBN. An easier way would be to repeat the washing procedure and remeasure the topography to see if the irregularities change or dissapear. This would mean the irregularities are a result of contamination or left over resist.

In order to optimise the patterning process by preventing the formation of ridges and/or irregularities, it is important to understand the origin of those features. AFM imaging in between each patterning step is needed to distinguish where in the process irregularities and/or ridges are formed and what they are. Topography information about the hBN surface prior to patterning and the surface of the resist after writing would be of particular interest for this purpose.
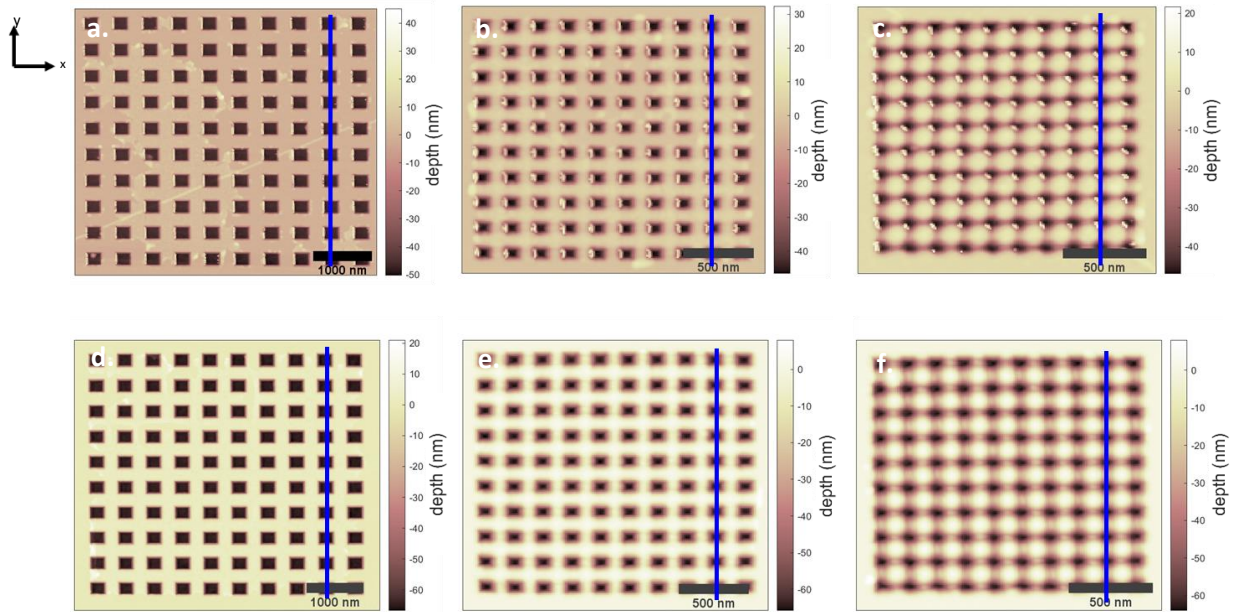
Figure 24: Surface topography images of square hole arrays patterned into hBN with pattern depths of 45 nm (a-c) and 65 nm (d-f). The targeted hole sizes are 250, 100 and 80 nm^2 for the topographies shown in a + d, b + e and c + f respectively. Cross sections (shown in Figure 25) were taken along the blue lines.

4.3.2.2 Overall Pattern Quality and the RMS Error

To further analyse the topography and pattern quality, we took cross sections along the blue lines in Figure 24. The cross sections through the topography of HA45 patterns are shown in Figure 25a, b and c for n is 250, 100 and 80 nm respectively. From a visual inspection of the cross sections, we can see that the targeted pattern (n is 250 nm) was reproduced well (with the exception of an outlier likely caused by a local patterning error). When n is decreased to 100 nm, the holes are still reproduced, but the pattern is more curved compared to the larger pattern. Upon further decreasing the targeted hole size (n is 80 nm), the periodicity of the holes remains. However, the height difference between the top and bottom of hole does no longer correspond to the targeted depth and the square shape of the wave breaks down. Furthermore, the RMS errors (as explained in section 2.3.2) were calculated to quantify how well the targeted pattern was reproduced into the hBN. The observations are consistent with the increasing RMS Errors with decreasing pattern size (6.2, 11.7 and 18.4 nm for the patterns with n is 250, 100 and 80 nm respectively).

The cross sections through the topography of HA65 patterns are shown in Figure 25d, e and f for n is 250, 100 and 80 nm respectively. The cross sections of the HA65 patterns are more curved compared to those in HA45, however the trends observed upon decreasing the targeted hole size are similar. The pattern with n is 250 nm is reproduced well, the pattern with n is 100 becomes more curved and the pattern with n is 80 reproduced the periodicity, but is no longer a square wave with the targeted amplitude. These observations are confirmed by the increasing RMS Errors with decreasing pattern size (9.7, 17.7 and 23.3 nm for the patterns with n is 250, 100 and 80 nm respectively).
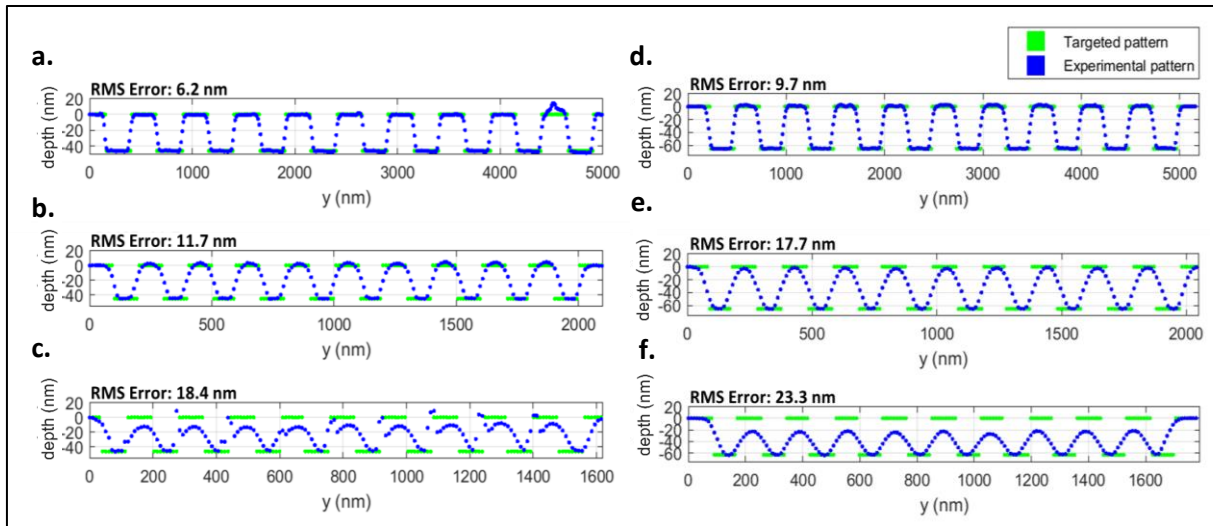
Figure 25: Cross section through the surface topography images of the square hole arrays patterned into hBN with pattern depths of 45 nm (a-c) and 65 nm (d-f). The targeted hole sizes are 250, 100 and 80 nm² for the topographies shown in a + d, b + e and c + f respectively. The experimental cross sections (blue) are plotted together with the targeted square waves (green). The cross sections were taken along the blue lines in Figure 24.
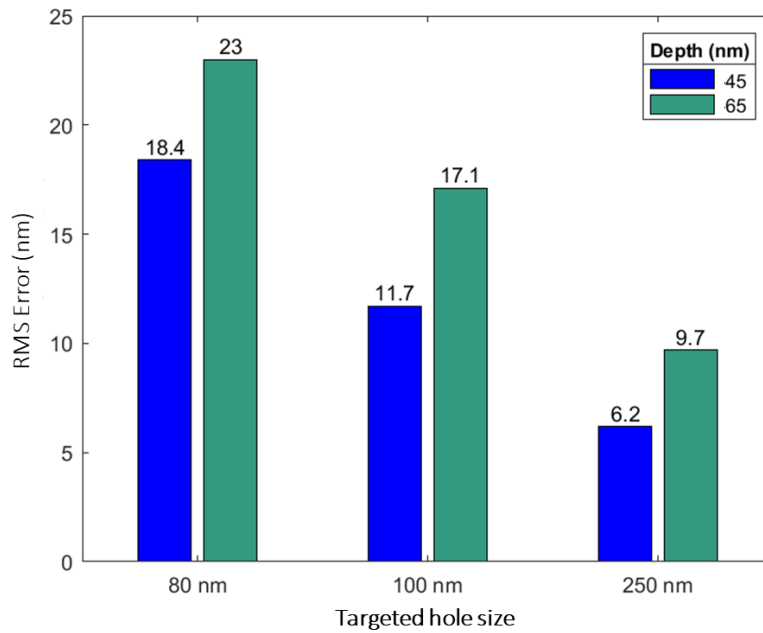
Figure 26: Bar diagram of the RMS errors between the measured topography and targeted patterns of square hole array with different depths and hole sizes.

To get a better understanding of the factors influencing the pattern quality, it is useful to compare the different RMS errors. Therefore, a bar diagram with the values of the RMS errors of the square hole array patterns with different sizes and depths is shown in Figure 26. In here, we observe two trends: first, as the targeted hole size increases, the RMS errors decreases. Second, the RMS errors are consistently larger for patterns with an increased depth. Further analysis with a larger variety of depths is needed to confirm this trend. Nevertheless, the apparent trend can be understood by the influence of the tip shape on the pattern as discussed in Theory section 2.3.2. When the depth of the pattern is larger, a larger part of the tip needs to contact the resist, therefore affecting the shape of the pattern more. Additionally, as the width of the hole becomes smaller the effect of the tip shape becomes relatively larger.

Thus, the influence of the tip shape appears to be the limiting factor in patterning precision. However, analysis of the surface topographies in between each patterning step is needed to confirm which patterning step is the limiting. Additionally, designing the future experiments such that the writing depth in the resist corresponds approximately to the pattern depth in the hBN (by writing the resist with shallower depths and adjusting the duration of the etching) will contribute to a better understanding of the limiting step.

Again, it should be noted that tip convolution during AFM measurements also affects the shape of the measured pattern (section 2.2.1). To remove the error caused by tip convolution, deconvolution of the measured topography should be performed which is challenging as the shape of AFM tip is unknown (see explanation in section 4.2.1.2). In future experiments, the AFM tip shape could be determined using SEM which could then be used to set the tip parameters for deconvolution.

Furthermore, depending on the patterning depth and feature size the targeted patterns were reproduced into hBN with RMS errors between 6.2 and 23 nm using the tSPL workflow. This is sufficient precision for some applications, nevertheless often nanometer precision is required.[27] Because the depth appears as the limiting factor (due to the tip shape), writing shallower patterns in the resist and/or depth enhancement techniques using etching selectivity[27] or a hard mask strategy[8] might offer a pathway towards increased precision. Notably, the precisions were obtained for patterns that were designed as binary, while the obtained patterns were often not binary but wavy. It is likely that an increased precision (and lower RMS error) would be obtained when writing patterns intentionally designed as wavey. Furthermore, the most important reason to use tSPL for hBN is that greyscale patterning enables more freedom in device design. Therefore, it would be interesting to perform further analysis on greyscale patterns, *e.g.* patterns with a sine function as cross section as was also suggested for further analysis on resolution in section 4.3.1.

Thus, as the size of features increases and the depth of the pattern is shallower, the pattern precision becomes lower. These observations indicate that the tip shape during the writing step could be the limiting factor, however additional experiments and analysis (especially on the topography of the patterned resist) are needed to confirm this. We obtained patterns with errors as low as 6.2 and 23 nm on patterns with a binary targeted shape and suggest depth enhancement techniques as a route towards increased patterning precision. Furthermore, we suggest further patterning precision analysis in hBN on greyscale patterns as that is one of the major strengths of tSPL.

5. Conclusion & Outlook

In this work, we investigated the capabilities and limitations of thermal scanning-probe lithography to (greyscale) nanostructure hexagonal boron nitride. Firstly, we were able to successfully transfer patterns from the resist into the hBN, including a pattern containing different depth levels (the Mandelbrot set pattern). Therefore, we conclude that the tSPL workflow used is a suitable method to enable greyscale patterning of hBN. For future research it would be interesting to see what the best obtainable vertical resolution is when patterning hBN using the tSPL workflow.

Secondly, we analysed the pattern quality of several patterns in terms of the following pattern characteristics: the minimum feature size, the resolution and the overall patterning precision. To analyse the minimum feature size we used the Mandelbrot set pattern which we characterised with AFM. The minimum feature present in the pattern had a FWHM of 40 nm with a depth of 40 nm. The shape of this feature corresponds to the shape of the probe tip used for tSPL, indicating that the tip shape is the limiting factor.

To analyse the resolution we used square hole arrays with depths of 45 an 65 nm, in which the highest resolution we found was ~100 nm. We determined the resolution by measuring the half-pitch of fully separated features (square holes in this case) with SEM images. Furthermore, the half-pitches found for the patterns with larger depth were consistently a bit larger compared to those with shallower depths. A possible explanation for this is the influence of the shape of the probe tip used for tSPL.

To quantify the overall patterning precision we used the RMS error between the targeted and experimental pattern. We managed to reproduce the targeted pattern (square hole arrays) into the hBN with an RMS error below 10 nm. We performed this analysis on binary square hole array pattens with different targeted half-pitches (250, 100 and 80 nm) and depths (45 and 65 nm). Upon decreasing the targeted half-pitch and increasing the depth of the pattern, the RMS error increased, which is possibly caused by the shape of the tip.

Our results clearly demonstrate the capability of the patterning of hBN using the tSPL workflow. Nevertheless, higher patterning qualities could be obtainable after further optimisation of the workflow. Our results indicate the tip shape of tSPL as the possible limiting step. If this is indeed the case shallower patterning in the resist and/or depth enhancement techniques might offer increased pattern qualities. Furthermore, under or over etching has a large influence on the pattern quality, so optimisation of the etching process could increase the quality of the patterns. Measuring and analysing the surface topographies in between each patterning step is needed to confirm the origin of quality limiting steps in the patterning process. The obtained information could then be used to further optimise the quality limiting steps.

Thirdly, we suggest further analysis of the capabilities and limitations of patterning hBN with the tSPL workflow on greyscale patterns. Higher pattern qualities might be obtained compared to the binary square hole arrays, because greyscale patterning is the strength of tSPL. For instance, patterns with a sine function as the targeted cross section could be used for such analysis. The amplitude (depth) and period (pitch) could be varied to enable a systematic analyses of the minimum feature size, resolution and overall patterning precision as function of depth and feature size.

In summary, we conclude that the tSPL workflow is capable of binary and greyscale patterning of hBN. Future research on the capabilities and limitations of nanostructuring hBN using tSPL should focus their efforts on greyscale patterns, a better understanding of the limiting step and improving the quality of patterning. Furthermore, as we found that tSPL is a suitable pathway for greyscale patterning of hBN increased freedom in the design of hBN containing nanodevices is enabled.

Acknowledgements

Lay Persons Abstract

Nanotechnology contains very small objects and devices and used in a wide variety of applications. For example, it can be found in batteries, solar cells and computer chips. Research towards nanotechnology focusses on the development of electronic and photonic devices on the nanoscale. It is built from nanomaterials with sizes from several hundreds of nanometres down to only a few nanometres, with one nanometer being a billion times smaller than one meter. For comparison, a nanometer fits about 100 000 times in the thickness of an average human hair.

One of the major reasons for the interest in nanomaterials and nanotechnology originates from the fact that the properties of nanomaterials are size and shape dependent. To illustrate how exceptional this is, you can think of any kind of daily material like a bar of chocolate. Changing the size of the chocolate bar will not change its colour or taste, while for nanomaterials it would. Therefore, the properties of nanomaterials can be tuned to make them suitable for applications in nanotechnology simply by shaping and/or structuring them.

Hexagonal boron nitride is an example of a nanomaterial that can be employed in nanotechnology due to its favourable properties like high stability (which means for instance that it can withstand high temperatures). Recently, by structuring hexagonal boron nitride advancements have been made towards further implementation in optical and electronic applications. However, current methods used for the nanostructuring of hexagonal boron nitride limit the design of nanodevices as they can only realise structuring in two dimensions (2D). Novel and improved device architectures could be realised when nanostructuring in three dimensions (3D) would be possible.

Thermal scanning-probe lithography is a technique capable of such 3D structuring of materials at the nanoscale. The way structuring with thermal scanning-probe lithography works is illustrated in Figure 27, where the material of interest (blue) is coated with a protective layer called the resist (grey). Firstly, the desired structure is engraved into the resist with a very small (as small as a few atoms) and hot needle (Figure 27a). When the heated needle and resist are in contact evaporation of the resist occurs at the location of contact, leaving an empty spot in the resist. The depth of the spot is determined by how far the needle is pushed into the resist, controlled by the amount of force exercised on the needle. By precisely regulating the force and the location of the needle, the shape of the remaining resist can be sculpted to any desired landscape. Secondly, once the desired landscape is engraved into the resist, the landscape needs to be transferred into the underlaying material of interest (Figure 27b). This is accomplished by bombarding the surface with reactive ions removing layers of material. The resist protects the material, but where the resist layer was engraved (and thus is thinner) the underlying material gets exposed. There, the layers of the underlaying material will also start to be removed. The amount of removed material at every location is determined by how long the materials is exposed which in turn is determined by the landscape in the resist. Therefore, the landscape is transferred into the underlying material.

In this work, we explored the suitability of this method for the structuring of hexagonal boron nitride. We found we could structure hexagonal boron nitride with sub-10 nm overall precisions and resolutions of 100 nm. This shows that thermal scanning-probe lithography is suitable for patterning of hexagonal boron nitride. For implementation in nanotechnology the precision could be improved further. After the analysis of different patterns with different sizes and depths, we hypothesise that the limiting factor in patterning precision is the shape of the tip. Furthermore, we demonstrated that 3D landscapes can be structured into hexagonal boron nitride using thermal scanning-probe lithography opening up a pathway towards improved and novel device architecture on the nanoscale.
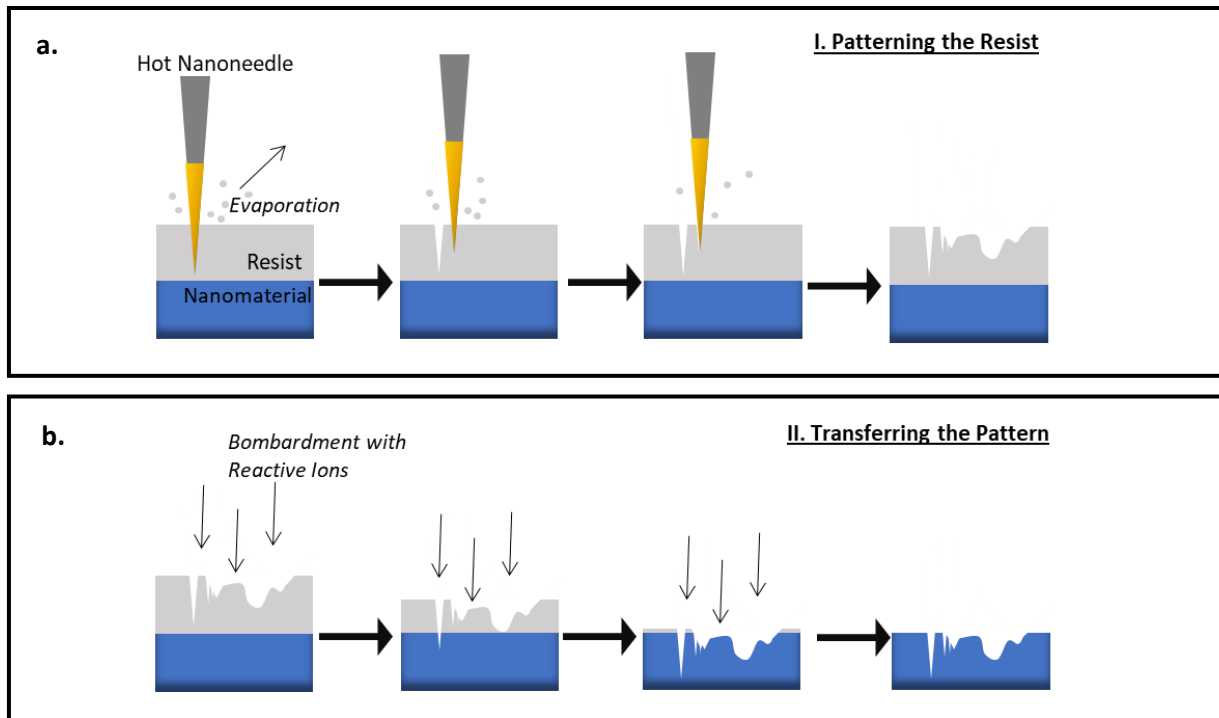
Figure 27: Side view of the working principle of nanostructuring a material using thermal scanning-probe lithography. a. The material that needs to be patterned (blue) is coated with a protective layer called the resist (grey). Firstly, the desired structure is engraved into the resist using a very small (as small as a few atoms) and hot needle. When the heated needle and resist are in contact in contact local evaporation of the resist occurs, leaving an empty spot in the resist. The depth and location of the needle are precisely controlled at each location in the resist, resulting in the desired structure. b. The pattern is transferred from the structure is transferred from the resist into the underlying substrate by bombarding the surface with reactive ions removing layers of material.

References

1. Caldwell, J. D. *et al.* Photonics with hexagonal boron nitride. *Nat. Rev. Mater.* **4**, 552–567 (2019).

2. Dean, C. R. *et al.* Boron nitride substrates for high-quality graphene electronics. *Nat. Nanotechnol.* **5**, 722–726 (2010).

3. Bhimanapati, G. R., Glavin, N. R. & Robinson, J. A. 2D Boron Nitride: Synthesis and Applications. in *Semiconductors and Semimetals* vol. 95 101–147 (Elsevier Inc., 2016).

4. Woessner, A. *et al.* Highly confined low-loss plasmons in graphene-boron nitride heterostructures. *Nat. Mater.* **14**, 421–425 (2015).

5. Jessen, B. S. *et al.* Lithographic band structure engineering of graphene. *Nat. Nanotechnol.* **14**, 340–346 (2019).

6. Ziegler, J. *et al.* Deterministic Quantum Emitter Formation in Hexagonal Boron Nitride via Controlled Edge Creation. *Nano Lett.* **19**, 2121–2127 (2019).

7. Garcia, R., Knoll, A. W. & Riedo, E. Advanced scanning probe lithography. *Nat. Nanotechnol.* **9**, 577–587 (2014).

8. Pires, D. *et al.* Nanoscale Three-Dimensional Patterning of Molecular Resists by Scanning Probes. *Science* **328**, 732–735 (2010).

9. Knoll, A. W. *et al.* Closed-loop high-speed 3D thermal probe nanolithography. *Altern. Lithogr. Technol. VI* **9049**, 90490B (2014).

10. Ryu Cho, Y. K. *et al.* Sub-10 Nanometer Feature Size in Silicon Using Thermal Scanning Probe Lithography. *ACS Nano* **11**, 11890–11897 (2017).

11. Howell, S. T., Grushina, A., Holzner, F. & Brugger, J. Thermal scanning probe lithography—a review. *Microsystems Nanoeng.* **6**, 1–24 (2020).

12. Lassaline, N. *et al.* Optical Fourier surfaces. *Nature* **582**, 506–510 (2020).

13. Fan, Y., Zhao, M., Wang, Z., Zhang, X. & Zhang, H. Tunable electronic structures of graphene/boron nitride heterobilayers. *Appl. Phys. Lett.* **98**, 1–4 (2011).

14. Proscia, N. V. *et al.* Near-deterministic activation of room temperature quantum emitters in hexagonal boron nitride. *Optica* **5**, 1128–1134 (2017).

15. Tran, T. T., Bray, K., Ford, M. J., Toth, M. & Aharonovich, I. Quantum emission from hexagonal boron nitride monolayers. *Nat. Nanotechnol.* **11**, 37–41 (2016).

16. Nikolay, N. *et al.* Direct measurement of quantum efficiency of single photon emitters in hexagonal boron nitride. *Optica* **6**, 1084–1088 (2019).

17. Chejanovsky, N. *et al.* Quantum Light in Curved Low Dimensional Hexagonal Boron Nitride Systems. *Sci. Rep.* **7**, 1–14 (2017).

18. Voigtländer, B. *Scanning Probe Microscopy - Atomic Force Microscopy and Scanning Tunneling Micrsoscopy*. *Surface Characterization: A User's Sourcebook* (Springer-Verlag Berlin Heidelberg, 2015).

19. Alessandrini, A. & Facci, P. AFM: A versatile tool in biophysics. *Meas. Sci. Technol.* **16**, (2005).

20. What is Atomic Force Microscopy (AFM). *NanoAndMore GMBH* https://www.nanoandmore.com/what-is-atomic-force-microscopy. Date last accesed: 30-04-2021.

21. Fenwick, O. *et al.* Thermochemical nanopatterning of organic semiconductors. *Nat. Nanotechnol.* **4**, 664–668 (2009).

22. Probes -> NCHV-A Overview. *Bruker* https://www.brukerafmprobes.com/p-3364-nchv-a.aspx. Date last accesed: 30-04-2021.

23. Raposo, M., Ferreira, Q. & Ribeiro, P. a. A Guide for Atomic Force Microscopy Analysis of Soft-Condensed Matter. *Mod. Res. Educ. Top. Microsc.* 758–769 (2007).

24. Canet-Ferrer, J., Coronado, E., Forment-Aliaga, A. & Pinilla-Cienfuegos, E. Correction of the tip convolution effects in the imaging of nanostructures studied through scanning force microscopy. *Nanotechnology* **25**, 1–9 (2014).

25. Kollipara, P. S., Li, J. & Zheng, Y. Optical Patterning of Two-Dimensional Materials. *Res. - A Sci. Partn. J.* **2020**, 1–15 (2020).

26. Altissimo, M. E-beam lithography for micro-/nanofabrication. *Biomicrofluidics* **4**, 2–7 (2010).

27. Rawlings, C. D. *et al.* Control of the interaction strength of photonic molecules by nanometer precise 3D fabrication. *Sci. Rep.* **7**, 1–9 (2017).

28. Cheong, L. L. *et al.* Thermal probe maskless lithography for 27.5 nm half-pitch Si technology. *Nano Lett.* **13**, 4485–4491 (2013).

29. Coulembier, O. *et al.* Probe-based nanolithography: Self-amplified depolymerization media for dry lithography. *Macromolecules* **43**, 572–574 (2010).

30. Moody, J. What does RMSE really mean? *Towards Data Sience - Medium* https://towardsdatascience.com/what-does-rmse-really-mean-806b65f2e48e (2019). Date last accesed: 20-05-2021.

31. Golla, D. *et al.* Optical thickness determination of hexagonal boron nitride flakes. *Appl. Phys. Lett.* **102**, (2013).

32. Singh, S. L., Prasad, B. & Kumar, A. Fractals via iterated functions and multifunctions. *Chaos, Solitons and Fractals* **39**, 1224–1231 (2009).

33. Devaney, R. L. Unveiling the Mandelbrot set. *Plus* http://plus.maths.org/content/unveiling-mandelbrot-set (2006). Date last accesed: 11-05-2021.